EPHEMERAL ACTIVE REGIONS AND CORONAL BRIGHT POINTS

A SOLAR MAXIMUM MISSION II GUEST INVESTIGATOR STUDY

(Final Report, NASA Grant NAS5-28728)

Principal Guest Investigator:

Karen L. Harvey
Solar Physics Research Corporation
4720 Calle Desecada
Tucson, AZ 85718

Guest Co-Investigator:

Frances Y. C. Tang
Big Bear Solar Observatory
264-33 Caltech
Pasadena, CA 91125

Guest Co-Investigator:

Victor Gaizauskas
Herzberg Institute of Astrophysics
National Research Council
100 Sussex Drive
Ottawa K1A OR6 CANADA

SMM/UVSP Co-Investigator:

Arthur I. Poland
Goddard Space Flight Center/NASA
Code 682
Greenbelt, MD 20771

Submitted by:

Karen L. Harvey
Solar Physics Research Corporation
May 17, 1986

EPHEMERAL ACTIVE REGIONS AND CORONAL BRIGHT POINTS

(A Solar Maximum Mission II Guest Investigator Study)

Abstract

The results of this investigation have confirmed a dominate association of coronal bright points (as seen in He λ10830) with the approach and subsequent disappearance of opposite polarity magnetic network. While coronal bright points do occur with ephemeral regions, this association is a factor of 2-4 less than with sites of disappearing magnetic flux. The intensity variations seen He I λ10830 are intermittent and often rapid, varying over the 3 minute time resolution of the data; their bright point counterparts in the C IV λ1548 and 20 cm λ show similar, though not always coincident time variations. Ejecta are associated with about one-third of the dark points and are evident in the C IV and Hα data.

These results support the idea that the anti-correlation of x-ray bright points with the solar cycle can be explained by the correlation of these coronal emission structures with sites of cancelling flux, indicating that, in some cases, the process of magnetic flux removal results in the release of energy. That the intensity variations are rapid and variable suggests that this process works intermittently.

1. Introduction

Coronal bright points were first identified in soft x-ray solar images as small scale emission structures of <30" with lifetimes of hours (Vaiana *et al.*, Golub *et al.*, 1974). Bright points since have been detected in the XUV (Sheeley and Golub, 1979), the EUV (Tousey *et al.*, 1972; Habbal and Withbroe, 1981) and more recently with the VLA at 20 and 6 cm wavelengths (Habbal *et al.*, 1986). Detailed studies of high resolution x-ray and XUV observations indicate the bright points consist of small loops that evolve on time scales of minutes. Coronal bright points were found to be spatially associated with small magnetic bipolar structures. The properties of these bipoles are identical to those observed in ephemeral active regions, i.e, they have characteristic dimensions of 10-15 Mm, an average total flux of $\sim 3 \times 10^{19}$ Mx, and lifetimes of the order of 8-12 hours (Golub *et al.*, 1977; Harvey and Martin, 1973; Harvey *et al.*, 1975). Both coronal bright points and ephemeral regions occur on the sun in large numbers (several hundred at any give time) over a broad range of latitude. The similarity in their properties suggested that ephemeral regions and x-ray bright points are correlated. In detailed comparisons with magnetic field observations, Golub *et al.* (1977), however, found that only about half of the x-ray bright points corresponded with identified ephemeral regions. In addition, as shown in Figure 1, the number of x-ray bright points varies 180° out of phase with the solar cycle variation of sunspots (Golub *et al.*, 1977; Davis, 1983) and also of ephemeral regions (Martin and Harvey, 1979; Harvey, 1984, 1985). Since their initial discovery, no simultaneous set of time-sequence x-ray and magnetic field observations have been obtained in order to investigate and clarify the connection between coronal bright points and ephemeral regions.

X-ray bright points are also correlated with similar-sized, but dark structures in He I D_3 and λ10830 spectroheliograms (Harvey *et al.*, 1975). This result suggested a possible way to study the association of these coronal emission structures and the evolution of the underlying photospheric magnetic fields. Using the National Solar Observatory full disk He I λ10830 observations, Harvey (1984, 1985) compared the locations of He I "dark points" with bipolar regions identified on daily full disk magnetograms as either ephemeral regions (new magnetic flux) or as a bipole resulting from the close approach of existing magnetic network of opposite polarity. It was found that a larger fraction of the He I λ10830 dark points, and presumably x-ray bright points, were associated with bipolar regions resulting from the encounter of existing, (apparently unrelated) magnetic network of opposite polarities than with ephemeral regions. This association led to a possible explanation of the anti-correlation of coronal bright points with the sunspot cycle. Encounters of opposite polarity network are more likely to occur in mixed polarities regions. Giovanelli (1979) determined the area of the sun covered by mixed polarity fields to vary anti-correlated with the solar cycle, as shown in the bottom plot in Figure 1. An overplot of the x-ray bright point counts (from Davis, 1983) shows a good correlation leading to the hypothesis that the solar cycle variation of x-ray bright points is dominated by the occurrence rates of encounters of opposite polarity network.

Since November 1984, a comprehensive set of observations has been collected as part of the Solar Maximum Mission Guest Investigator Program to investigate the properties and changes in the magnetic fields associated with He I λ10830 dark points and bright points observed in the transition region and corona. Participating in these collaborations were six ground-based observatories providing time-sequence, high-spatial resolution observations in the quiet sun of the photospheric magnetic fields, longitudinal and transverse components, Hα, He I λ10830 spectroheliograms, 20 and 6 cm λ radio maps and two Solar Maximum Mission instruments obtaining observations in C IV, Si II, He II, O VIII, and Ca II. Coronal bright points were identified using He I λ10830, C IV, O VIII, 20 and 6 cm λ images, and compared with the magnetic field pattern measured directly or inferred from Hα structures and with the velocity field deduced from Hα, C IV, Si II line profiles.

This report describes the observations obtained during six observing periods in 1983-1985, and the analysis and comparison of these data sets. As shown in the following sections, we are able to answer some of our basic questions regarding the associations of coronal bright points and the underlying magnetic field in the quiet sun. But as with many studies, unexpected and very exciting results were found that will be intensively followed up in the near future. These will be discussed briefly in Section 5 of this report.

2. Observations

Six ground-based observatories and two SMM instruments obtained data during all or part of a total of five observing efforts in 1984 and 1985. The observations from a sixth observing effort between the National Solar Observatory and Big Bear Solar Observatory during October 10-12, 1983 has been included in this study. The following sections discuss each participating observatory, the Co-Investigator contacted at each observing site to coordinate the scheduled observing runs, the types and statistics of observations obtained.

2.1. *National Solar Observatory* (NSO), K. Harvey:

He I 10830 spectroheliograms were made of a 512"x512" area using the 512 channel magnetograph (Livingston *et al.*, 1976) at the Vacuum Telescope on Kitt Peak. Spatial resolution (instrumental) is 1"; area scans were repeated every 3 minutes during the observing day, yielding 70-120 images per day. To view and analyze these data, the spectroheliograms were converted into displayed images on an interactive computer system at National Optical Astronomy Observatories (NOAO) and video taped to make a movie. This medium allowed a easy avenue to study the data and to identify dark points, their evolution and associated phenomena that would not have been seen in an image by image analysis. Some technical difficulties were experienced in this procedure. First encountered was a long delay for the software to process the observations; this was implemented early last winter. Second, the recording heads on the video disk system, used to construct the video movie, were wearing out, resulting in noise being added to the recorded video images. The system finally failed before all of the λ10830 data was processed. The data from one day remains to be converted.

2.2. *Big Bear Solar Observatory* (BBSO), F. Tang:

A video magnetograph (Zirin, 1985) was used at the 25cm refractor in the Ca I λ6103 line to obtain measurements of the longitudinal component of the photospheric magnetic field ($B_{\parallel}$). An integration of 1024, 2048 and 4096 pictures per magnetogram was used for the 1983, 1984, and 1985 magnetograph data, respectively. Sensitivity and noise (comparable to the sensitivity) is estimated for each integration at 10 G for 1024 integrations, 5 G (2048 integrations) on 28 November, 20G (also 2048 integrations) on 9 December, and 2.5 G for 4096 integrations used in the 1985 data. A single area of ~4.2′x5.6′ was observed in the 1983 (Oct 10 and 11) and in 1984; time resolution of these data ranged from 2-5 minutes depending on the integration time per magnetogram. For the Oct 12, 1983 and 1985 observations, BBSO sequentially observed four areas around the target coordinates (~8′x11′) allowing better coverage of the region of the sun monitored by NSO. This worked well to increase the area of observation and the statistics of "events" of interest, but decreased the time resolution to around 25-30 minutes. Hα center-line filtergrams were also obtained of the same area as the magnetic field observations.

A 16mm copy of the Hα and magnetic field data was converted to a video tape movie format for analysis at the NOAO facilities. As with the He I data, this task was not completed due to equipment failure. About six days of data remain to be processed.

2.3. *Ottawa River Solar Observatory* (ORSO), V. Gaizauskas:

Hα filtergrams were obtained using a 0.25Å Zeiss filter at Hα line center and displaced 0.3Å, 0.4Å, 0.6Å, 0.75Å, and 1.0Å symmetrically to the red and the blue. These data have a spatial resolution is 1-3". A complete scan through the wavelength sequence took ~45 seconds to complete. ORSO observed an area of 4′x5′, moved to cover an area 8′x10′ centered on the target coordinates; this decreased the time resolution for any given area to about 3 minutes. Because the observatory is not open during the winter months, ORSO obtained observations only for the 1985 coordinated runs.

2.4. *Marshall Space Flight Center* (MSFC), M. Hagyard:

Longitudinal ($B_{\parallel}$) and transverse [B_T] magnetograms were made with a video vector-magnetograph using the Fe I λ5250 line (Hagyard *et al.*, 1984, 1985). The field of view

was 5.7′x5.7′ with spatial resolution of 2.5" The longitudinal magnetograms took 2 minutes to complete and were repeated at 3-6 minute intervals. The transverse field measurements took 10 minutes and were interspersed among the $B_{\parallel}$ observations. Magnetic field sensitivity is estimated at 4 G for $B_{\parallel}$ and 150 G for B_T.

2.5. *Solar Maximum Mission, Ultraviolet Spectrometer and Polarimeter* (UVSP), A. Poland:

The UVSP instrument and capabilities have been described by Woodgate ***et al.*** (1980). The principal set of data from this experiment are line profiles (the intensity measured at 5 positions in the lines from -.3 to +.3 Å) of C IV λ1548.19 and Si II λ1533.43 made during one orbit on 28 November 1984 and six consecutive orbits on 9 December 1984; spatial resolution is 10" and the observations were repeated at a rate of 6.8 minutes giving between 4-8 rasters per orbit. A spectroheliogram in the He II λ1638.3 during the first orbit on 28 November and a C IV spectroheliogram on 9 December had a spatial resolution of 3" over an area of 4′x4′.

2.6. *Solar Maximum Mission, Flat Crystal Spectrometer* (FCS), J. Saba, K. Strong:

The FCS (Acton ***et al.***, 1980) operated in a raster mode and a "sit and stare" mode to obtain spectroheliograms in the O VIII λ18.969 line (formed at 2.5-3 x 10^6). In the raster mode, an area 4′x4′ was scanned in 10" steps with a spatial resolution of 15". In the "sit and stare" mode, the integrated intensity of one pixel positioned on a bright structure was measured. Because we expect the features we are trying to detect in O VIII are weak, if visible, based on a study by Tang ***et al.*** (1983), the data are going through special processing to maximize the signal to noise ratio. This is discussed in more detail in Section 3.5.

2.7. *Very Large Array (VLA): 20 and 6 cm λ Maps*, S. Habbal:

Solar radio maps were acquired for only the 8-9 September 1985 observing effort using the VLA at 20 cm λ on 8 September and at 6 cm λ on 9 September. The 20 cm data has a spatial resolution of 16", and the 6 cm, 6". Analysis of the radio data in this study has been restricted to the that obtained on 8 September, since no simultaneous He I λ10830 spectroheliograms were made on 9 September due to cloudy weather. The initial data reduction and processing of the radio data has been done by Shadia Habbal and Robert Ronan.

2.8. *Swarthmore College*, R. Holt:

Ca II line profiles were taken in bright structures corresponding to He I λ10830 dark points. Specific targets were selected on the basis of 10830 spectroheliograms transmitted to R. Holt and discussions near the beginning of each observing day. Holt's study is being done independently of this investigation and will not be discussed further in this report.

In 1983, 1984 and 1985, six observing programs were carried out during (1) 10-12 October 1983, (2) 28 November 1984, (3) 9 December 1984, (4) 25-28 May 1985, and (5) 25-27 June 1985, and (6) 8-9 September 1985. The hours observed are listed in Table I along with the center position of the selected area and an indication of the type of area observed: QS = quiet sun and CH = coronal hole. During May 1985, the coronal hole was fairly weak and small, so much of the area was quiet sun (QS+CH).

Table I. Observing Times of Participating Observatories

Observatory	1983			1984		1985								
	10 Oct S06W01 QS	11 Oct S05W14 QS	12 Oct S28E26 CH	28 Nov N09W07 CH	9 Dec S05E19 CH	25 May N01W51 CH	26 May N23E33 CH & QS	27 May N23E19 CH & QS	28 May N23E02 CH & QS	25 Jun N00E06 QS	26 Jun N00W07 QS	27 Jun N00W21 QS	8 Sep N00E00 QS	9 Sep N00E00 QS
NSO	1734-2308	1756-2219	1846-2212	1745-2130	1906-2258	1906-2535	2037-2520	1752-2438	1824-2215	1604-2234	1811-2530	1630-2325	1604-2234	-
BBSO	1824-2319	1613-2233	1715-2319	1859-2043	1742-2225	1538-2438	1630-2503	1658-2520	1639-2504	1535-2449	1457-2514	1447-2147	1714-2452	1558-2324
ORSO				-	-	1318-1845	1342-1738		1727-2223	-	-	1441-1751	1438-1922	
MSFC				1840-2057	1640-1827	1624-2314	1617-2245	1608-2243	-	-	-	-	1618-1947	1636-2004
VLA													1631-2115	1600-2400
SMM, UVSP				1828-1849 2000-2034	1539-1354 1709-1735 1843-1915 2018-2056 2152-2236 2326-2424									
SMM, FCS				1825-1901 2000-2039	- - -	1900-1948 2031-2122 2205-2259	2009-2058 2009-2059 2141-2233		1746-1826 1917-2003 2952-2141	1548-1648 1722-1822 1857-1957 2031-2131 2205-2305 2340-2440	1832-1931 2006-2106 2141-2240 2315-2414	1807-1906 1942-2039 2116-2215	1627-1657 1801-1836 1935-2017 2110-2158 2244-2338	1602-1630 1736-1810 1911-1951 2045-2139 2219-2311

3. Data Analysis and Results

In this section, the analysis and comparison of the data sets obtained in the six coordinated observing runs is discussed. Each of the data sets is considered separately, beginning with the He I λ10830 observations, and then is compared with other data.

3.1. *He I λ10830 Observations*

He I λ10830 is a chromospheric absorption line produced by transitions of the He I triplet from the 2^3S to the 2^3P energy levels. It is formed in the chromosphere at a temperature of 7,000 K at about the same height as Hα. The He I triplet has a higher population than is expected from chromospheric temperatures, and it has been suggested that the excessive population is produced by recombination following photoionization of He I by coronal EUV radiation of λ<500 Å (Goldberg, 1937). In such a model, dark structures in He I λ10830 result from the excitation of overlying EUV/x-ray emission (such as in coronal bright points) and He I coronal holes (bright areas with little or not network visible) from the lack of coronal EUV/x-ray excitation. Consistent with this explanation, Harvey *et al.* (1975) found a good correlation between x-ray bright points and similar sized dark structures in He I D_3 and He I λ10830. Since soft x-ray images are not available to identify and study coronal bright points, we have used the 'dark points' observed in He I λ10830 as a coronal bright point proxy.

Quickly apparent in the He I λ10830 movies of the quiet sun and coronal holes is a dynamic and rapidly changing chromosphere. The large intensity variations in He I absorption both in time and space, appear to be more readily visible in He I than can be seen in Hα, where most events are of equal magnitude in intensity changes and scale to already very variable chromosphere. The Hα "galloping chromosphere" (Sawyer, 1974) occurs at a reduced level in He I.

3.1.1. NETWORK VARIATIONS

When viewing the movies of the He I λ10830 data, one sees in a slightly darker network pattern, a low level (~10%), small-scale (a few arc sec) variation in intensity. This variation is almost oscillatory in appearance and gradually decreases as one move toward the limb. It disappears at longitudes 45°, suggesting that this intensity variation may be due to the motions of spicules, fibrils associated with the network.

3.1.2. DARK POINTS

He I 'dark points' are defined for this study as a dark structures with a mean intensity at least 25% greater than the surrounding network regions and a sizes ranging from 5" to 30". Three examples of He I 'dark points' seen in λ10830 are shown in Figures 2, 3a and 3b. We find they are not spatially uniform in intensity, but show considerable variation and often several centers of enhancement (darkening) within what is identified as the dark point. The spatial structure and overall intensity varies in as short a time interval as 3 minutes, the time resolution of the observations.

We see two times scales in the intensity variations in what is defined as a He I dark point: (a) an isolated, rapid darkening, reaching a peak in 3-10 minutes, and lifetimes of 20-30 minutes; An example is shown in Figure 2, and (b) a longer-lived (hours) structure that can show considerable variation in intensity over its lifetime, as shown in Figures 3a and 3b. The lifetimes of the longer-lived dark points generally exceeded the observing interval, i.e., they were greater than 6-8 hours. These structures often displayed

intensity variations similar to the rapid dark points; these events occur from an already enhanced state in the dark point which differs from the rapid dark points, which develop at sites of no enhanced He I λ10830 absorption. For these events, we adopt the term "dark point flares", because of their similarity with their x-ray and EUV counterpart. The decay of the dark point "flares", both in the rapid dark points and the longer-lived structures, appears to be nearly as fast as the rise of the event. In many cases, the end of a dark point, such as shown in Figure 3b, is marked by the occurrence of a dark point "flare", a behavior also seen in x-ray bright point flares (Nolte ***et al.***, 1979; Sheeley and Golub, 1979) and in their EUV counterparts (Habbal and Withbroe, 1981).

For 5 of the days observed, the occurrence rate of the rapid dark points per hour per 10^{10} km^2 and the areal density (in units of 10^{10} km^2) of long-lived dark points is shown in in Table II.

Table II. Areal Density of He I Dark Points (DP)

	1984		1985		
Rapid DP/10^{10} km^2/hr	0.44	0.54	0.77	1.12	0.72
Long-Lived DP/10^{10} km^2	2.66	1.94	3.71	3.85	4.94

3.1.3. EJECTA

It was noticed in the He I movies that associated with many of the rapid darkenings were ejecta. These are manifested in several ways in the He I data.

Frequently, small-scale, bright structures are seen in the He I λ10830 spectroheliograms, such as is shown in the bottom panel of Figure 4. The bright structure indicated by the arrow appears at 2124, replacing a dark point seen on the previous frame, and is visible on two frames or for at least 3 minutes. Such structures are typically 4-8 arc sec in size. They are seen generally only on one spectroheliogram, so their lifetimes are probably $\leq$3 minutes. Because of the way the He I λ10830 observations are made, these bright structures have been interpreted as a velocity structure. The He I spectroheliograms are made with one slit of the magnetograph in centered on the He I λ10830 line and the second positioned in the 'continuum' to the red side. The signal recorded is the difference between the intensity in the two slits divided by their sum. (This is the method used to determine velocities with the magnetograph, only for the He I λ10830 line the slits are not centered on the line.) If the line profile of a feature is significantly velocity shifted, the structure will appear 'bright' in the spectroheliograms. (The velocity at which this occurs, assuming the line profile shape does not change, is estimated at 20 kms^{-1}. During the 3.87 hours of observations on 9 December 1984 and the 6.5 hours on 8 September 1985) counts of these bright structures were made. 127 bright structures (or 2.47/hr/10^{10} km^2) were identified in the 9 December 1984 data and 276 (or 3.91/hr/10^{10} km^2) in the 8 September 1985 data. This is equivalent to about 2000 such events per hour on the surface of the Sun assuming a 3 minute lifetime.

The development of the dark points with rapid, large intensity variations shows, in many cases, a directed expansion of the absorption structure. This expansion generally is restricted to an angle of $<25^\circ$. Such is the case in the event shown in the sequence of He I pictures in the top panel of Figure 4. The appearance is surge-like and occurs during the rapid increase in in the dark point absorption. The time scale and behavior of these events is similar to that described by Moore ***et al.*** (1977) for macrospicules and associated x-ray bright point 'flares'. For 6 of the days analyzed, this type of ejecta event accompanied 76 (33%) of 229 He I rapid dark points and 42 (17%) of the 245 long-lived dark points. The average rate of occurrence of these ejecta within the areas observed is $0.32/hr/10^{10}$ km^2. This is a factor of three higher than found by LaBonte (1979) for macrospicules detected in Hα near sunspot minimum of the last solar cycle. LaBonte, however, has cautioned that the counts of macrospicules are dependent on the observing technique employed to detect them.

Perhaps related to these ejecta are the eruption of small scale (10,000-30,000 km in extent) filaments. Such an event is shown in Figure 5; a filament becomes visible in He I 10830 around 1740 UT, though it is easily visible in Hα before this. The filament grows stronger in Hα and in He I λ10830, finally erupting at 1905 UT, accompanied by a darkening of the adjacent He I dark point (see the intensity curve in Figure 3a) and a brightening of the nearby Hα plage (though of shorter duration than in He I). This event occurs at a time when there is a substantial loss of magnetic flux at southern footpoint of the filament. Several of these events have been detected in the He I data, however, without Hα, it is difficult to distinguish filaments at this scale from nearby dark network or a dark point. Hermans and Martin (private communication) are studying these events using the BBSO large scale Hα and magnetic observations. They find that, on average, one filament eruption occurs per day in their field of view. For an 8 hour day, this is equivalent to 0.06 events/hr/10^{10} km^2.

A forth type of ejecta seen in the He I λ10830 data is illustrated in Figure 6a. It is associated with a rapid dark point or dark point flare in He I followed by the ejection of a dark, front-like arch-shaped diffuse cloud. The angular extent of the disturbance is generally 60-100°, though in a few cases it has been seen over an angle of nearly 270°. This differs from the surge-like ejecta described above in its annular extent and in the distance it can be detected. The intensity peak in the associated dark point is not necessarily very dark as is found in the other types of ejecta noted in this discussion; the duration of the initiating dark point also is short, 6-15 minutes. These disturbances propagate with horizontal velocities ranging from 16-140 kms^{-1} over distances from 20,000-70,000 km. As seen in Figure 6b, the two events, shown in Figure 6a, have velocities of 16 and 53 kms^{-1}. Such ejecta were detected in 23 (10%) of the 229 rapid dark points and 7 (3%) of the 245 longer-lived dark points. The average rate of occurrence of these ejecta is $0.10/hr/10^{10}$ km^2. Propagating disturbances associated with coronal bright points may have been detected in the EUV and the cm λ radio data (Habbal, private communication).

In some instances, the disturbance itself is not seen, but followed after the occurrence of a rapid dark point with ejecta characteristics by a succession of rapid dark points along the projected direction of the initial ejecta. Such a situation may be the case with the occurrence on 12 October 1983 of the four dark points shown in Figure 7. The position of each dark point has been plotted at the time of the beginning of its darkening. They fall fairly close to a straight line of a velocity 57 kms^{-1}. While is it difficult to prove that a "propagating disturbance" produced the succession of dark point events

on 12 October, the fact that such disturbances can be seen in He I is suggestive. The propagation distance in the 12 October case is about 200,000 km, much greater than seen in those events where a disturbance is visible. However, similar cases of the successive, possibly related occurrences of several distant dark points have been in coronal holes and over similar distances. Statistical studies will be done to test if this is a real phenomenon or due to coincidence.

Some of the characteristics of these events are similar to the small scale filament eruptions. However, there appear to distinct differences. All of the small scale filaments become visible in He I λ10830 and darken considerably from 10-90 minutes before erupting. In most of the events associated with propagating disturbances, no such increase in absorption is seen. Often the associated dark point only darkens a little though the event is quite rapid (rise time ~3-6 minutes). The angular extent of the events is much greater for some events than is usually seen in filament events. It, however, is not clear what the propagating disturbances are. Definitely a subject for future study.

3.2. *Magnetic Field Observations*

The principle set of magnetic field observations used in this study was taken at the Big Bear Solar Observatory using their video magnetograph. For the 1983 and 1984 data (with the exception of one day) only one area was observed during the scheduled runs. For the remainder of the observations, four adjacent areas were observed sequentially about the target coordinates. There is some overlap in the individual fields of view so that the magnetic field pattern over the extended area could be constructed. During the six observing runs, 3 different integrations were used: 1024 for the October 1983 data, 2048 for the 1984 data, and 4096 for the 1985 data. Because the sensitivity and noise level changes with the different integration levels, the identification of emerging magnetic flux, disappearance of flux, and the association with phenomena in He I 0830 has been considered separately for the data of each integration.

The BBSO magnetic field and Hα data was converted from 16mm to video movie format to be analyzed at the NOAO facilities. This job could not be completed because of the failure of a necessary piece of equipment. Thus, only 8 of the days studied could be analyzed in a movie format; the remainder (6 days) of the magnetic field observations have been examined using prints of the magnetograms at made at 2-3 hour intervals.

Sections of the BBSO magnetograms are shown in Figures 8-14. The magnetic field is displayed as a series of concentric alternating patterns of black and white; a turn over from black to white or white to black indicates the field has saturated at that integration level. The outer color indicates the polarity of the field; white designates positive magnetic flux and black, negative. The magnetic fields observed in the quiet sun are comprised of network fields, generally stronger, more stable structures, and of intranetwork fields. Over a several hour period, the network fields change shape, divide, spread out, contract, join with other network; the general pattern of network, however, remains recognizable on this time scale. The intranetwork fields are weak. They appear at or near the center of magnetic network cells, and migrate to the boundaries to either cancel with opposite polarity network or join network of the same polarity (Livi *et al.*, 1985; Zirin, 1985). Also seen in these data are many cases of "sinks" of magnetic flux, i.e., locations where magnetic network and intranetwork fields move toward and disappear.

Of particular interest in this study is the emergence of ephemeral regions and

encounters of already existing magnetic network of opposite polarities. Ephemeral regions were identified in the data as magnetic bipoles that emerge during the observations. Initially, they appear as a close pair of opposite polarity poles ~5000 km in extent. The magnetic poles of ephemeral regions strengthen and separate. This definition allows us to separate emerging bipolar or multipolar intranetwork structures, which are weaker and tend to migrate differently, from ephemeral regions. Several examples of the emerging ephemeral regions are shown in Figures 8, 9, 10 and 12.

The locations of opposite polarity network encounters are defined as network that over a period of time approach to within a few arc sec and in most cases exhibit a loss of magnetic flux. The disappearance observationally of magnetic flux between two opposite polarity structures has been termed cancelling flux by Livi ***et al.*** (1985). Most approaching opposite polarity poles result in the mutual disappearance or cancelling of their flux. However, this is not always detected within the time frame of the observations, even though the opposite polarity poles remain in close proximity (i.e., within a few are-sec) for many hours. Observations suggest that even though there may not be flux disappearing in this situation, the two opposite network elements have become magnetically connected and, therefore, may be of significance in an association with He I dark points. In this discussion, we will use a more general term "magnetic flux encounters" to describe situations where (a) opposite polarity magnetic flux approaches and merges and (b) where two magnetic poles (ephemeral regions excluded) are in close proximity, not separating, and no obvious flux loss is observed. The term cancelling flux is used to designate the mutual loss of magnetic flux in the encounter of opposite polarity network. In Table III, the number of ephemeral regions (ER) and encounters of opposite polarity network (ϕ Enc.) is tabulated for the 3 days in 1983, 2 in 1984 and 4 days in 1985. For the reasons stated in Section 2.2, the results are divided into the three periods shown, based on the number of integrations used in the magnetic field observations (1024, 2048, and 4096). We expect these numbers will change when all the magnetic field observations are analyzed with the movie format.

Table III. Number of ER and Magnetic ϕ Encounters

	Number of Integrations		
	1024	2048	4096
	1983 data	1984 data	1985 data
Ave. Area (10^{10} km^2)	2.30	3.80	14.40
Number of ER	131	9	191
Number of ER/10^{10} km^2/hr	3.27	0.47	0.46
Number of ϕ Enc	146	20	211
Number of ϕ Enc/10^{10} km^2/hr	3.70	0.91	0.51

The positions and timing of ephemeral regions and of magnetic flux encounters were compared with the He I λ10830 spectroheliograms to establish the correlation with the development and evolution of He I dark points and associated phenomena. This association was both varied and complex; many sites of emerging magnetic flux showed no evidence of dark points in He I, while rather minor appearing magnetic field changes in terms of the flux involved, (both emerging and disappearing flux), seemed to be associated with spectacular darkenings and ejecta in the λ10830. Several examples of this association are shown in Figures 8-13 and illustrate the variety of phenomena seen in He I λ10830 accompanying similar magnetic field changes observed in the photosphere. In Figure 8, a large ephemeral region (total flux=6×10^{19} Mx) emerged, at location "1", 3.5 hours before a diffuse, dark structure developed in He I λ10830. The He I structure occurred coincident with the addition of magnetic flux into the region and the formation of an arch filament system in Hα (visible in the last pictures in Figure 8). No He I dark point or structure was associated with the emergence of an almost equally large ephemeral region near the active region shown in Figure 9. The dark point that developed formed between the region's negative pole and the nearby positive flux in the active region. This event typifies what often is observed in the association of ephemeral regions and dark points. Many dark points are correlated not with the ephemeral region itself, but with the approach and cancellation of the flux of one pole of the ephemeral region with nearby opposite polarity network. Marsh (1977) also found this to be true in associating Hα microflares observed in the quiet sun with ephemeral regions. In Figure 10, white (positive) magnetic flux appears and increases between two strong black (negative) network structures and almost as quickly decreases and disappears. Coincident with this, a rapid dark point and ejecta occur in He I λ10830 positioned over positive flux and the left (east) negative polarity network. The ejecta is directed as shown by the arrow. The peak of the He I dark point seems to occur near the maximum in the positive magnetic flux (within the time resolution of the magnetic field observations ~25 min.). The time scale of this magnetic event was much more rapid than is usually seen and occurs on a small spatial scale; it is possible that as the positive flux is emerging (strengthening in the observations), it also is cancelling with the adjacent negative polarity network.

As is apparent in the previous discussion and examples, the association of He I dark points is better correlated with the approach, encounter and mutual cancellation of opposite polarity magnetic network than with emerging flux. A dark point may persist for the entire duration of the encounter of the opposite polarity flux, be seen for only a short time, or if a longer-lived structure, fade hours before the magnetic flux has disappeared. The He I λ10830 event shown in Figure 11 was a rapid, extensive event that occurred once. It spread within 3 minutes around the boundaries of a supergranular cell, inferred from the network and magnetic field pattern. It was associated with a positive pole (white) at the arrow moving toward and encountering a line of negative network. Ejecta occurred near the event's onset. The longer-lived dark points associated with magnetic flux encounters often show sporadic or intermittent intensity variations during their lifetime, e.g., features 2 and 3 in Figure 8 and the dark points in Figure 12 (intensity curve, Figure 3b) and Figure 13. (The dark point in Figure 13 was observed in C IV and is discussed in more detail in Section 3.4.) These dark points can persist for the duration of the magnetic flux cancellation (such as in Figure 12), but will often disappear before the magnetic event is over (such as feature 3 in Figure 8). For all of the dark points that are seen to develop during the simultaneous He I λ10830 and magnetic field observations,

they appear only when the distance between the borders of the approaching opposite polarity magnetic network are less than a few arc-sec (<5"). In Hα, connecting fibrils and small filaments form between the approaching poles (see feature 2, Figure 8; Figure 9), indicating reconnection may be taking place between these apparently unrelated network magnetic structures.

For almost 40% of the He I dark points, no change in the longitudinal component of the magnetic field could be seen. Such an example is shown in Figure 14; the rapid dark point with ejecta occurred with no detectable change in the magnetic field. This particular event was the second of four shown in Figure 7.

Table IV is a tabulation showing the association of rapid dark points (DP, rapid) and long-lived dark points (DP, L-L) and He I ejecta with identified ephemeral regions (ER) and magnetic flux encounters (ϕ Enc.). In Table V, the reverse correlation is tabulated, i.e., the number of ephemeral regions and magnetic flux encounters associated (or not) with He I dark points and ejecta.

Based on these results, we conclude that not every ephemeral region or magnetic flux encounter will be associated with a dark point in He I λ10830. Magnetic flux encounters are more likely to be associated with a dark point and with dark points with ejecta than ephemeral regions. Between 2-4 times as many dark points occur at sites of encounter of opposite polarity magnetic flux, suggesting that the cancellation and the formation of a magnetic connection between existing magnetic network is a more likely environment for the heating of the atmosphere overlying these magnetic structures. A higher fraction of the rapid dark points are not associated with observed magnetic field changes than is seen with the longer lived dark points. This suggests that the rapid variations in intensity in dark points may be related to more dynamic magnetic field changes occurring above the photosphere over a relatively short time scale that are not reflected in the photospheric magnetic observations.

3.3. *Hα Observations*

The Hα filtergrams taken by BBSO have been used to get some idea of the direction of the horizontal or transverse component of the magnetic field in the chromosphere and to determine the magnetic connections (and their development) between network of opposite polarities. In much of our data set, the association of Hα features and Hα events with He λ10830 structures is a difficult assessment to make using the BBSO data. One reason is that the 1985 Hα data, where the seeing is quite good, have a time resolution of ~25 minutes. Events in Hα take place over a much shorter time scale than the magnetic field, and we undoubtedly miss many phenomena and are unable to follow some of the more interesting aspects of the association with He I λ10830 events. This phase of the analysis has been restricted to specific events in the 1985 data and to the data that provides good time resolution (1983 and 1984).

The filament eruption shown in Figure 5 illustrates an event seen both in Hα and He I λ10830, as well as the correlation of Hα bright network with He I dark network. There is a general association between the locations of Hα and He I network, though it is not one to one. He I structures of often more extensive than their Hα counterparts. This is due to the appearance of the fibrils, spicules, filaments, and network as dark often unresolved structures in He I λ10830. In some instances specific structures can be identified, like, for example, the filament in Figure 5. This filament can be seen in Hα

Table IV. Percentage of Dark Points Associated with Magnetic Field Changes

	1983	1984		1985		Total Number of Events
DP, Rapid with ER	17%	10%	9%	9%	17%	76
DP, L-L with ER		8		20		
DP, Rapid with ϕ Enc.	48	19	34	25	39	162
DP, L-L with ϕ Enc.		48		33		
DP, Rapid with No $B_{\parallel}$ Change	36	71	57	63	55	246
DP, L-L with No $B_{\parallel}$ Change		43		47		
Total Number of Events	107	44		333		484
DP & Ejecta with ER		6%		12%		13
DP & Ejecta with ϕ Enc.		38		36		41
DP & Ejecta with No $B_{\parallel}$ Change		56		52		59
Total Number of Events		16		97		113

Table V. Percentage of Magnetic Field Changes Associated with Dark Points

	1983	1984		1985		Total Number of Events
ER with DP, Rapid	27%	11%	55%	8%	36%	98
ER with DP, L-L		44		28		
ER with No DP	73	45		64		200
ER with DP, Ejecta		11		8		13
ϕ Enc. with DP, Rapid	53	6	82	22	70	191
ϕ Enc. with DP, L-L		72		48		
ϕ Enc. with No DP	47	18		30		114
ϕ Enc. with DP, Ejecta		24		26		41
Total Number of Events	276	26		301		603

before its appearance in He I λ10830 about one hour before it erupts. This has been seen in other such events and suggests that the changing environment of the filament that leads to the eruption may also cause the enhanced He I λ10830. Associated with this filament eruption was a rapid darkening in the He I beginning at 1852 that lasted for about one hour (see the intensity curve in Figure 3a). While a brightening of the adjacent Hα network also occurred (see the Hα filtergram at 1905 in Figure 5), its duration was much shorter than seen in He I λ10830. For a some of the ejecta events in He I λ10830, we see in Hα the appearance or extension of long fibrils (macrospicules?) and their abrupt disappearance. No simultaneous observations of the He I small-scale bright structures, thought to be velocity structures, nor of the propagating disturbances have been found in the BBSO data to date.

As part of this collaborative observing program, filtergrams were obtained a several positions in the Hα line from +1Å to -1Å by the Ottawa River Solar Observatory. The detailed comparison of the He I λ10830 and Hα data, which will give us information about mass motions in the chromosphere, is just beginning. Our first look at these data have indicated some intriguing relations that will be pursued using more of the data in the coming months. Six events in 8 September 1985 He I λ10830 observations have been selected to determine the association with Hα structures and velocities. The positions of these six events are shown in Figure 15. Table VI is a list of the features, their identification in He I λ10830, the magnetic field change and the associated velocity structure in Hα.

Table VI. Comparison of the Six Events in Figure 15

Event Number (see Figure 15)	He I Event	$B_{\parallel}$ change	Hα event
1	dark point, filament	none	small filament that fades
2	dark point, variable	cancelling flux	complex small-scale activity and velocities
3	rapid dark point	cancelling flux	none
4	dark point, variable	cancelling flux	possible changes
5	bright "velocity"* structure	none	none
6	bright "velocity"* structure	none	none

*in He I, a bright (3-6") structure interpreted as a velocity, see Section 3.1.

In feature "1", minor velocities <10-15 kms^{-1} are seen in Hα from 1657-1715 UT, simultaneous with the darkening of a filament in He I λ10830. The geometry of this flow has not been established at this stage of the analysis, but it may be either axial or a slight downflow at ends and upflow in the filament's center. The weak velocity flow gradually disappears by 1715, as the filament fades in He I. More intriguing is feature "2", associated with the approach and merging of opposite polarity network and a He I λ10830 dark

point. In He I λ10830 a dark point is evident and strong at the beginning of the observations at 1604 UT. During the next 2 hours, it is variable in intensity with a sharp increase in absorption beginning at 1658 UT, reaching a peak at 1715 UT. In Hα, this outburst is not accompanied by a brightening of the network in core of the line. However, at 0.6Å off line center, rapidly changing structures are visible in both wings, each showing considerable and different fine structure down to the resolution limit of the observations. These have been tentatively identified as small scale mass motions showing a complicated pattern confined to within the boundaries of feature 2. A second similar, but less strong, event occurs in Hα about 30 minutes later near the time of a second rapid darkening in feature "2". The timing of the two Hα events, shown in Figure 16, indicates a close temporal relation with the rapid intensity variations seen in this particular He I dark point.

In the next few months, this aspect of the study will be continued in great detail and expanded to include several other He I events of interest.

3.4. *C IV Observations*

During the 28 November 1984 and 9 December 1984 observing efforts, simultaneous observations were obtained with the Solar Maximum Mission UVSP instrument in the lines of C IV, Si II and He II. The principle data set considered in this section is the line profile observations taken in the C IV line at 1548.13 Å. Observations were made at five positions in the C IV and Si II lines, from -0.3 to +0.3 in 0.15Å increments. A 4′x4′ area was rastered at each line position, building up a measure of the line profiles in the two lines every 6.8 minutes in a 24 x 24 array with a 10" spatial resolution. These data were transferred to the NOAO computer, where the line profiles were fitted with a least squares gaussian to determine a line shift, corrected for space craft velocity, the peak line intensity, and line width at each point in the raster. We have no measurement of the actual position of the C IV line, but assume it to be as 1548.13Å. Several strong velocities (>60 kms^{-1}) are seen in these maps; the line profiles at these locations were not guassian, resulting in a poor fit to the line profile model. The velocity determinations and errors will be studied carefully and using different methods discussed in a study of C IV UVSP data by Klimchuk (1986).

The C IV data were then compared with the He I λ10830 observations to determine the correlation between He I and C IV structures and to identify velocity flows in the transition region with He I dark points and ejecta. In Figure 17, a comparison is shown for three He I λ10830 spectroheliograms and the corresponding C IV intensity and velocity maps of an area in a coronal hole observed on 9 December 1984. We find an excellent correlation between the structures that are dark in He I and bright in C IV. For several events in the He I data, we are examining the C IV intensities and velocities; two events are described here. The first event occurs at the left edge of the area shown in Figure 17. In He I this feature darkens quite rapidly beginning at 2151 UT, just before the first C IV observation. The dark point peaks at 2157, decays rapidly, and is almost gone by 2209 UT. The intensity variation in C IV is similar with a strong bright point at the first observation at 2157 UT, that is weakly visible at 2209. At 2203 UT, a bright structure, interpreted as velocity, is appears in the dark point; it is more easily seen in Figure 17 in an enlargement of the area. In C IV, a blue shifted velocity flow of 15-25 kms^{-1} over an area 20"x30" exactly overlies the He I velocity structure and dark point. This velocity feature can be detected only in the one C IV raster, however, the precise correspondence

of this feature with the velocity structure in He I suggests that the velocity flow is real. This phase of the analysis is still going on, so statistics are not available on the extent of the association between the velocities measured in C IV and He I dark points or events.

The He I dark point "B" (Figures 17 and 18) is associated with the approach of two opposite polarity network elements (shown in Figure 13). A comparison between the intensity variations observed in C IV and He I for feature B is shown in Figure 19. Unfortunately, there were no strong intensity variations in the 10830 dark point during the C IV observations. However, the intensity variations seen in the C IV bright point seem to correspond to smaller variations seen in He I, like, for example, the peaks occurring 2034 and 2206 UT.

Many of the C IV bright points are associated with encounters of opposite polarity magnetic network, though there were not many ephemeral that emerged in the UVSP area during these observations. This results does not contradict the results of Tang ***et al.*** (1983), where the two observed C IV λ1548 bright points were at the locations of ephemeral regions. Both of those ephemeral regions also involved the magnetic flux encounters when one of the region's poles migrated into nearby opposite polarity network.

3.5. *O VIII Observations*

The processing of the O VIII data taken with the Flat Crystal Spectrometer on board SMM has run into several difficulties. A software bug which caused gaps in the data during processing, and improvements to increase the signal to noise ratio, very necessary in trying to detect what we expect to be very weak structures, if visible at all, are being tried. The software problem has been fixed and a background algorithm is being reconsidered, though there now exists one sufficient for an initial processing of the data. To try to improve the signal-to-noise ratio, several avenues are being explored: the use of a new, more sensitive background subtraction (4-sec averages), choosing a contouring scheme interactively to maximize signal-to-noise, improving statistics by adding adjacent pixels, then successive rasters, then both.

The following procedure has been established with Julia Saba (private communication) for reduction and analysis of the data:

(1) Two days have been selected when FCS observing mode was repeated 4′x4′ images (initial days considered 25 May and 26 June 1985). This allows study of variability and raster summation for improved the signal to noise ratio.

(2) The remaining observations of 4′x4′ raster sequences will then be analyzed.

(3) We will then consider the observations of a 4′x4′ raster followed by the "Sit and Stare" bright point mode (an integrated intensity measured in one pixel centered on the brightest point in the 4′x4′ field of view; look for variations in integrated flux measurements at location of bright point.

(4) The remaining data will be analyzed.

If a bright point is obvious in individual images (with or without pixel summation), temporal variations will be looked for. If bright point is not obvious after adding pixels and rasters, upper limits will be computed at bright point coordinates determined on the basis on the He I dark point positions.

3.6. *20 cm λ Radio Observations*

At 20 cm wavelength, the radio emission from bright points arises mainly from heights typical of the low corona-transition region. On 8 September 1985, simultaneous observations of the quiet sun were made in He I λ10830, 20 cm λ, $B_{\parallel}$, and Hα. The correspondence found between the compact (20-40") radio sources observed at 20 cm with the VLA and the He I λ10830 dark points is shown in Figure 20. The radio bright points with a dashed and a solid contour are those observed to last longer than 2 hours in the ~5 hours of simultaneous observations. Most of the 20 cm bright points coincided with He I dark points, though there are more dark points than radio sources. Comparisons with high resolution magnetograms confirmed that the radio bright points (and He I counterparts) overly bipolar regions. Seven of 11 bright 20 cm points being studied in detail are located at sites of disappearing magnetic flux resulting from the encounters of existing opposite polarity magnetic flux; in two 20 cm bright points, magnetic flux is both emerging and disappearing, and in the remaining two, there is no obvious change seen in the magnetic field.

The changes in time of the maximum radio brightness temperature and the mean intensity of the absorption in He I λ10830 are shown for four He I dark/20 cm bright structures in Figures 21a and 21b. These features are identified in Figure 20. We see sporadic variations in the emission (and absorption) occurring at the shortest time interval (3 min.) These variation are significant when greater than 10% of the He I λ10830 intensity and greater than 10^4 K in the radio brightness temperature). As can be seen in Figures 21a and 21 b, the temporal changes in the simultaneous observations are often correlated like in feature 1, 2, (Figures 21a) and 3 (Figure 21b). All of these features were associated with magnetic flux encounters, though in feature 1, emerging flux was also seen. The peak in the intensity curves for Feature 1 around 1900 UT is related to the eruption of a small scale filament (described in Sections 3.1.3 and 3.4). The peaks in intensity at 20 cm seem to occur after that reached in He I λ10830. The radio emission and He I absorption are not always correlated. A good example is in feature 4, where the large spike in the 20 cm data has no counterpart in the He I data. The He I intensity peak at 1954 UT appears to correspond with a similar peak in the radio data; however, the overall increase in 20 cm intensity is not mirrored in the He I observations. This may be related to the emergence of a bipole just south of the disappearing flux associated with feature 4 (as shown in Figure 12). The location of the peak intensity of 20 cm shifts southward during this increase. No similar increase in the He I λ10830 intensity at this location was noted.

4. Summary and Conclusions

While the analysis and comparison of the data sets taken during the six observing periods in 1983, 1984 and 1985 are still going on, several results and conclusions have been made regarding the correlation between He I λ10830 dark points (and presumably their x-ray/EUV counterpart) and the evolution of the photospheric magnetic field, Hα, C IV and 20 cm λ. These are summarized in this section. In the next section, there is a brief discussion of the work be completed under this study and of future studies that have resulted from this investigation.

The results from this study are as follows:

1. The network visible in He I 10830 displays a low level (<10%) intensity variation over a spatial scale of the order of arc-seconds and a time scale of minutes. These intensity variations are oscillatory in appearance and decrease toward the limb, almost completely disappearing at longitudes $>50°$, suggesting that the observed variations may be due to the motions of spicules and fibrils in the network.

2. He I 'dark points' have a characteristic size of 10-30 arc sec and intensity variations that show a variety of time scales from minutes to several hours. Two types of localized darkenings that occur in He I 10830 are defined as dark points: (1) a rapid darkening having a duration of about 10-30 minutes and often appears to be associated with ejecta, and (2) a longer lived darkening lasting hours, but which often shows large intensity variations (50-120%) on a time scale of minutes similar to the rapid dark points (these we identify dark point "flares", consistent with the similarly termed intensity variations in x-ray and EUV bright points).

There is a excellent correlation between the bright points observed in C IV and in 20 cm λ and the locations of He I λ10830 dark points. For many of the He I, C IV and 20 cm structures, similar intensity variations are seen, both in the long and short time scales. Though in some cases we find that the magnitude and phase of the the intensity variations (above the noise) are not consistent between 20 cm and He I.

3. Ejecta occur with 31% (113) of the 10830 rapid dark points and dark point "flares" occurring in the longer-lived dark points. These ejecta have been identified as surge-like macrospicules, small-scale filament eruptions, propagating disturbances of some type, and a bright "velocity" structures in He I. The propagating disturbances (associated with 6% of the dark points) are seen as a slightly darker, front-like arch-shaped, outward moving cloud in 10830 or as a successive darkening of several structures along a directed path consistent with the direction of an ejection from the initial dark point. These disturbances have horizontal velocities ranging from 16-140 kms^{-1} and travel over distances from 20,000-200,000 km. The bright structures, interpreted as a predominately vertical velocity structure, are small (3-6 arc sec) bright features in the He I λ10830 spectroheliograms. Their lifetimes are estimated as $\leq$3 minutes. If the average rates of occurrence of these ejecta are indicative of the whole sun, the number of ejecta per hour over surface of the Sun is:

Macrospicules and Filament Eruptions	197
Propagating Disturbances	62
Bright "Velocity" Structures	1964

We have not as yet identified in Hα a velocity structure corresponding to the bright "velocity" structures in He I. C IV λ1548 blue shifted velocity flows have been found at the sites of surge-like ejecta in He I λ10830. Complex small scale mass motions in Hα have been detected during the occurrence of He I dark point flares at a cancelling flux site.

4. All of the 484 He I dark points (both rapid and long-lived) are spatially associated with magnetic bipoles. 40% of these occurred at sites of magnetic flux encounters, i.e., encounters of existing, apparently unrelated opposite polarity network (in most cases, cancellation of the magnetic flux occurred); 14% were co-spatial with ephemeral regions that have emerged during the observing period. No change was seen in the underlying magnetic fields for 46% of the dark points. 37% of the 113 ejecta events occurred at the sites of encounters of opposite polarity magnetic flux, 9% with ephemeral regions, and for 54% no change in the magnetic field was detected.

In the correlation of magnetic field changes with He I dark points, 68% of the 346 disappearing magnetic flux sites were associated with He I dark points and 39%, almost a factor of two less, of 298 ephemeral regions that emerged were associated with a dark point. No dark point occurred for 32% of the magnetic flux encounters and 61% of the ephemeral regions.

5. For those dark points associated with magnetic flux encounters, the onset of the darkening seen in He I begins when the separation of the boundaries of the approaching opposite polarity network elements is <3-5 arc-sec. In Hα, connecting fibrils or a small filament form between these approaching opposite polarity features.

The characteristics and behavior of He I λ10830 dark points are very similar to those of coronal bright points observed in soft x-rays, the XUV and EUV wavelengths, suggesting that we are indeed studying the He I counterpart to the small-scale coronal emission structures. From a comparison with the underlying photospheric magnetic field, we find statistically that He I dark points and ejecta events are more likely (by a factor of 2-4) to be associated with encounters of existing opposite polarity flux than with the emergence of magnetic bipoles. Conversely, magnetic flux encounters are almost two times more likely to result in an associated dark point in He I than ephemeral regions. Not all ephemeral regions and encounters of opposite polarity magnetic network have a corresponding He I dark point. The high association of these features with significant changes in the underlying photospheric magnetic fields suggests that the magnetic field is playing an important role in the observed dynamic behavior of the He I dark points (and coronal bright points). The short-time scale of the intensity variations observed in He I λ10830, 20 cm and C IV suggests that the response is rapid to these dynamic effects. We conclude that energetic processes are connected with the removal of magnetic flux from the photosphere and to a lesser extent with emerging magnetic flux in the form of bipolar regions, though not in all cases. The rapid, sporadic variations seen in He I λ10830, C IV, 20 cm λ and Hα indicate that this process is not constant, but that it occurs intermittently. The formation of fibrils and small filaments between approaching opposite polarity network suggests reconnection may be taking place. Heating from intermittent magnetic field reconnection may explain the sporadic nature of the variability in absorption in dark points seen in the chromosphere and their bright counterparts in the transition region and corona.

The correlation of He I λ10830 dark points with specific magnetic field patterns and changes shows a dominate association with the approach and encounter of magnetic network of opposite polarity. This result supports the hypothesis suggested by Harvey (1984, 1985) that the number of x-ray bright points varies 180° out of phase with the sunspot cycle is due to their being more closely associated with magnetic flux encounters

rather than with ephemeral regions.

5. Work to be Completed

As is evident in this report, work is still in progress in several phases of this study of coronal bright points and the evolution of the underlying photospheric magnetic field. Over the next few months, we hope to complete this investigation and publish several papers as a result of this work, as follows:

1. Movies of the remaining He I λ10830, magnetic field and Hα data will be completed. These data will then be analyzed for the association between He I dark points and magnetic field changes. The Hα data will also be examined to establish, for a larger sample, what is taking place in the chromosphere related to He I ejecta, the magnetic flux encounters, and ephemeral regions. (with F. Tang, V. Gaizauskas)

2. The analysis of the C IV and Si II data will be completed; studied in detail are the velocity structures observed in these lines and how they relate to ejecta and events in He I λ 10830 and Hα, and the intensity variation correspondence. (with A. Poland)

3. The 20 cm λ data will be compared with the He I λ10830 observations to try to determine what distinguishes He I dark points with 20 cm counterparts with those without them. We will examine in more detail the intensity variations observed in the dark/bright points to understand why differences are seen for some events. At least one more collaborative observing run will be undertaken within the year to obtain simultaneous data in the 6 and 20 cm λ, He I λ10830, of the magnetic field and Hα. (with S. Habbal)

4. A detailed analysis will be continued comparing Hα velocity structures, determined from a series of filtergrams taken at several positions in the Hα line, with dark points, dark point flares and ejecta observed in He I λ10830. We are interested, particularly, in identifying the Hα counterpart to the bright "velocity" structures and the propagating disturbances seen in the He I data. Also to be studied in more detail are the small-scale mass motions that are observed within the boundaries of dark points and dark point flares.

5. The analysis of the O VIII data will continue to determine if we see coronal bright points at the site of He I λ10830 dark points.

6. Papers Published and in Preperation

Papers Published:

"The Association of Chromospheric and Coronal Phenomena with the Evolution of the Quiet Sun Magnetic Fields", K. L. Harvey, F. Tang, V. Gaizauskas, A. Poland, extended abstract for the Proceedings of the Workshop on Corona Plasmas and Prominences (held April 1985 and April 1986), in press.

"Simultaneous Observations of Changes in Coronal Bright Point Emission at the 20 cm Radio and He I 10830 Wavelengths", S. Habbal and K. Harvey, contribution to be published in the Proceedings of the Workshop on Corona Plasmas and Prominences (held April 1985 and April 1986), in press.

Papers in Preparation:

"The Association of Chromospheric and Coronal Phenomena with the Evolution of the Quiet Sun Magnetic Fields", K. L. Harvey, F. Tang, V. Gaizauskas, A. Poland, M. Hagyard.

"Simultaneous Observations of Changes in Coronal Bright Point Emission at the 20 cm Radio and He I 10830 Wavelengths", S. Habbal, K. L. Harvey, G. Hurford, R. S. Ronan, and G. L. Withbroe.

"The Association of Hα Velocity Events Observed in the Quiet Sun with He I λ10830 Dark Points and Ejecta", K. L. Harvey and V. Gaizauskas.

7. References

Acton, L. W., Culhane, J. L., Gabriel, A. H., and 21 co-authors:1980, *Solar Phys.* **65**, 53.

Davis, J. M.:1983, *Solar Phys.* **88,** 337.

Giovanelli, R. G.:1979, *Solar Phys.* **77**, 27.

Goldberg, L.:1937, *Astrophys. J.* **89**, 673.

Golub, L., Krieger, A. S., Silk, J. K., Timothy, A. F., and Vaiana, G. S.:1974, *Astrophy. J. Letters,* **197**, L133.

Golub, L., Harvey, J. W., Krieger, A. S., and Vaiana, G.:1977, *Solar Phys.* **53**, 111.

Habbal, S. R. and Withbroe, G. L.:1981, *Solar Phys.* **69**, 77.

Habbal, S. R., Ronan, R. S., and Withbroe, G. L.:1986, *Astrophys. J.*, in press.

Hagyard, M. J., Cumings, N. P., and West, E. A.:1984, in the Proceedings of the International Workshop on Solar Physics and Interplanetary Traveling Phenomena, Chin Biao (ed.), held in Kunming, China, November 1984, in press.

Hagyard, M. J., West, E. A., and Cumings, N. P.:NASA TH-82568, February 1985.

Harvey, J., Krieger, A.S., Timothy, A.F., and Vaiana, G.S.:1975, *Observazioni e Memorie Osservatorio de Arcetri,* **104,** 50.

Harvey, K. L.:1984, "Solar Cycle Variation of Ephemeral Active Regions", *Proceedings of the Fourth European Meeting on Solar Physics - 'The Hydromagnetic of the Sun'*, held in Noordwijkerhout, The Netherlands, 1-3 October 1984, **ESA SP 220,** 235.

Harvey, K. L.:1985, *Australian J. Phys.* **38**, 875.

Harvey, K. L. and Martin, S. F.:1973, *Solar Phys.* **32**, 389.

Harvey, K. L., Harvey, J. W., and Martin, S. F.:1975, *Solar Phys.* **40**, 87.

Klimchuk, J. A.:1986, PhD Thesis, University of Colarado, p. 63.

LaBonte, B. J.:1979, *Solar Phys.* **61**, 283.

Livi, S. H. B., Wang, J., and Martin, S. F.:1985, *Australian J. Phys.* **38**, 855.

Livingston, W. C., Harvey, J., Slaughter, C., and Trumbo, D.:1976, *Appl. Optics* **15**, 40.

Marsh, K. A.:1977, *Solar Phys.* **59**, 105.

Martin, S. F. and Harvey, K. L.:1979, *Solar Phys.* **64**, 93.

Moore, R. L., Tang, F. Bohlin, J. D., and L. Golub:1977, *Astrophys. J.* **218**, 286.

Nolte, J. T., Solodyna, C. V., and Gerassimenko, M.:1979, *Solar Phys.* **63**, 113.

Sawyer, C.:1974, *Solar Phys.* **35**, 63.

Sheeley, N. R., Jr. and Golub, L.:1979, *Solar Phys.* **63**, 119.

Tang, F., Harvey, K., Bruner, M., Kent, B., and Antonucci, E.:1983, *Adv. Space Res.,* **2,** No. 11, p. 65.

Tousey, R. J., Bartoe, J. D. F., Bohlin, J. D., Brueckner, J. D., Purcell, J. D., Scherrer, V. E., Sheeley, N. R., Jr., Schumacher, R. J., and VanHossier, M. E.:1973, *Solar Phys.* **33**, 265.

Vaiana, G. S., Krieger, A. S., Van Speybroeck, L. P., and Zehnpfennig, T.:1970, *Bull. Am. Phys. Soc.* **15**, 611.

Woodgate, B. E., Tandberg-Hanssen, E. A., and 12 co-authors:1980, *Solar Phys.* **65**, 73.

Zirin, H.:1985, *Australian J. Phys.* **38**, 961.

Figure Captions

Figure 1: Shown in the top plot from 1970 through 1984 are the variations of Ephemeral Regions (∗) [Harvey, 1985] compared the Sunspot Numbers (•) [Solar Geophysical Data]. In the bottom plot are the variations X-ray Bright Points (•) [Davis, 1983] compared with the fractional area of the Sun of mixed polarity regions (∗) [Giovanelli, 1979] from 1970 to 1981. Sunspot maximum and minimum are indicated by a tall and a short arrow, respectively.

Figure 2: The variation of the mean intensity in He I λ10830 during the occurrence of a rapid dark point that occurred in a coronal hole on 12 October 1983. He I spectroheliograms are shown at four times during this event. The scale of the pictures is 43,350 km in the east-west direction. The dark point at maximum (1929 UT) is 16,700 km along it longest extent. For all of the figures, North is at the top and east to the left unless otherwise specified.

Figure 3a: The variation of the mean intensity in He I λ10830 during a 4.5 hour period on 8 September 1985 of a long-lived dark point that shows at least two dark point flares. The largest of the events occurs around 1900 UT and is associated with the eruption of a small scale filament (shown in more detail in Figure 5). The pictures in the east-west (left-right) direction are 40,400 km.

Figure 3b: The variation of the mean intensity in He I λ10830 during a 4.5 hour period on 8 September 1985 of a long-lived dark point with two dark point flares. Following the last flare, which was accompanied by bright velocity structure seen in the fifth picture, the dark point faded. The pictures in the east-west direction are 37,200 km.

Figure 4: Two types of ejecta seen in He I λ10830 associated with dark points. ***Top sequence***: a surge-like expansion of the dark point, possibly a macrospicule. ***Bottom sequence***: the bright feature seen at 2124 is interpreted as a velocity structure. It is weakly visible at 2127 and gone by 2130. The size of the structure at 2124 UT is 6".

Figure 5: A sequence of Hα filtergrams (top) and He I λ10830 spectroheliograms showing the eruption of a small scale filament. The magnetogram at 1728 indicates the position of the filament (hatched area) relative to the fields. One footpoint (the southeastern) is in a white (positive) pole that is disappearing. The magnetogram and Hα data are taken by BBSO.

Figure 6a: Sequences of He I λ10830 illustrating propagating disturbances associated with the occurrence of two dark points. The arrow in the top sequence points to the front-like feature, moving out from a dark point beginning at 2246 UT. At 2255 UT the disturbance is both bright and dark. The horizontal velocity of this structure is 53 kms^{-1}. The bottom sequence of spectroheliograms shows a similar event that took place on 25 June 1985. Again, the arrow points to an arch-shaped expanding front, which moves out at a velocity of 16 kms^{-1}. The distance-time plots of these two events are shown in Figure 6a.

Figure 6b: The distance-time plots of the two propagating disturbances shown in Figure 6b.

Figure 7: The sequence of four He λ10830 spectroheliograms shows the positions of four dark points that occurred in succession, possibly as a result of a propagating disturbance initiated by the first dark point, "A", at 1902 UT. The onset times of the four dark points as a function of their position from dark point "A" are plotted in the distance-time plot below. Time runs from right to left in thik plot. The horizontal velocity of through the four points is 57 kms^{-1}. The distance between "A" and "D" is 195,000 km.

Figure 8: Sequences of Hα filtergrams (top), photospheric longitudinal photospheric magnetic fields (middle), and He I λ10830 spectroheliograms (bottom) of an area of the quiet sun on 11 October 1983. The magnetic field is displayed as a series of concentric alternating pattern of black and white; the polarity is defined by the outer ring, white is positive, and black negative. The structure labeled '1' is an ephemeral region which emerged during our observations. It had no associated He I λ10830 dark point until 3.5 hours after the region became visible in the magnetic field observations. This region had an arch filament system by 2150 UT, at which time a dark structure developed in He I. Structure "2" shows the approach and encounter of two opposite polarity network poles. At 2014 UT, the two poles are <6" apart; a dark point has formed at the $H_{\parallel}$=0 line between the two poles, and in Hα fibrils are seen to connect the two poles. Structure '3' apparently is the result of an ephemeral region that emerged near white (positive) network before our observations began. Magnetic flux cancellation occurs between the negative pole and the adjacent positive network. A dark point overlies this structure and the adjacent network. Over the course of the observations, the dark point fades. The Hα and magnetic field data were taken at the Big Bear Solar Observatory.

Figure 9: The darkening in He I λ10830 is associated with the migration of the negative pole of an ephemeral region into the positive magnetic fields of a nearby active region. The arrows in the 1927 UT pictures indicates the position of the ephemeral region, that emerged around 1845 UT, and in the 2139 UT and 2212 UT pictures, the location of the magnetic flux encounter. Hα fibrils connect the active region's positive fields with the approaching negative pole of the ephemeral region as early as 2045 UT.

Figure 10: Sequences of Hα filtergrams (top), photospheric longitudinal photospheric magnetic fields (middle), and He I λ10830 spectroheliograms (bottom) of an area of the quiet sun on 8 September 1985. The magnetic field is displayed as described for Figure 9. The arrows indicate the site of emerging (strengthening) positive magnetic flux located between two strong negative network elements. The rapid decrease in the positive flux indicates cancellation of the magnetic flux may be taking place. Simultaneous with this magnetic field change, a rapid He I dark point occurs with ejecta (the direction indicated by the thin arrow at 2142 UT). A dark structure is seen in Hα at 2154 offset to the north-west 7" extending in the direction of the He I ejecta. However, due to the low time-resolution of the data, it is not clear if it is associated with the He I ejecta. The Hα and magnetic field data were

taken at the Big Bear Solar Observatory.

Figure 11: Sequence of Big Bear Solar Observatory magnetograms (left) and He I λ10830 spectroheliograms (right) showing the occurrence of a very rapid dark "point" associated with the approach and encounter of network of opposite polarities. Though the merging of the magnetic poles continues for some time, only one event was seen in the He I data.

Figure 12: Sequence of Big Bear Solar Observatory magnetograms (top) and He I λ10830 spectroheliograms (bottom) showing a longer-lived dark point in He I associated with the disappearance of the underlying magnetic fields (at arrows). The dark point could not longer be seen after 2000 UT, when the positive network had disappeared. In the lower portion of the area shown, an ephemeral region emerged adjacent to negative network between 2007 and 2046 UT. Little He I darkening was associated with this event (at the arrowhead), though possibly a 20 cm λ bright point occurred with it.

Figure 13: Sequence of Big Bear Solar Observatory magnetograms (top) and He I λ10830 spectroheliograms (bottom) showing a long-lived dark point in He I associated with the approach of the opposite polarity network on 9 December 1984. This structure was also seen in C IV (see section 3.4. and Figures 17, 18 and 19).

Figure 14: Sequence of Big Bear Solar Observatory magnetograms (left) and He I λ10830 spectroheliograms (right) showing the location of a rapid dark point relative to the photospheric magnetic fields. No change in the field occurred at or near the time of the He I event. (This is one of the four events shown in Figure 7). The dark point indicated by the arrow is 16,700 km in extent. Earth north is at the top and east to the left.

Figure 15: Three Hα filtergrams from the Ottawa River Solar Observatory at ±.6 Å and center-line Hα of an area of quiet sun on 8 September 1985. Shown are the locations of six structures for which we tried to identify Hα velocity structures that might correspond to ejecta and events in He I λ10830. For two, feature "1" and feature "2" mass motions have been detected.

Figure 16: The mean intensity in He I dark point corresponding to feature "2" in Figure 15. The hatched strips indicate the timing of identified small scale mass motions occurring within the boundaries of the He I dark point located at feature '2'. The small scale activity in Hα, visible only in the wings, appears to be associated with the occurrence of "flares" in the dark point. The opposite polarity network underlying these structures is disappearing.

Figure 17: A sequence of three He I λ10830 spectroheliograms (top), and the corresponding C IV λ1548 center line intensity (middle) and velocity maps in C IV (bottom) of an area within a coronal hole observed on 9 December 1984. The pictures are 240"x240"; for these data North to the right and East to the top. As can be seen in the comparison, there is an excellent correlation between dark structures (dark points and network) seen in He I and the bright structures in C IV. C IV bright point "A" and a blue shifted velocity structure (arrow) are spatially and temporally

associated with a He I rapid dark point with ejecta.

Figure 18: A He I 10830 spectroheliogram at 2203 UT on 9 December 1984. Feature A and Feature B correspond to Features A and B on Figure 17. North is at the top and East to the left, this is rotated clockwise 90° from Figure 17. At the arrow is a bright structure next to the He I dark point; it is interpreted as due to a velocity shift associated with the rapid darkening at this location. The C IV velocity structure (at 2203 UT in Figure 17) is located precisely over the He I bright structure. The East-West distance is 273".

Figure 19: An plot of the mean intensity of Feature B (Figures 17 and 18) measured in C IV (dashed line) and in He I λ10830 (solid line). Vertical lines have been drawn between C IV and He I peaks at 2034 and 2234 UT.

Figure 20: A He I λ10830 spectroheliogram on 8 September 1985. The area shown is 512"x512". The locations of bright points identified in 20 cm λ maps are shown in relation to He I. Almost all of the 20 cm bright points are correlated with dark points in He I λ10830. The 20 cm bright points encirled by both a dashed and a solid line last more than 2 hours, the solid line <2 hours.

Figures 21a and 21b: Comparison of the mean intensity measured in He I λ10830 (solid lines) with the peak brightness temperature of 20 cm (dashed lines) for four of the He I dark points associated with 20 cm bright points. The four points are identified on Figure 20. The He I intensity is plotted on an inverse scale for easier comparisons.

Figure 21a

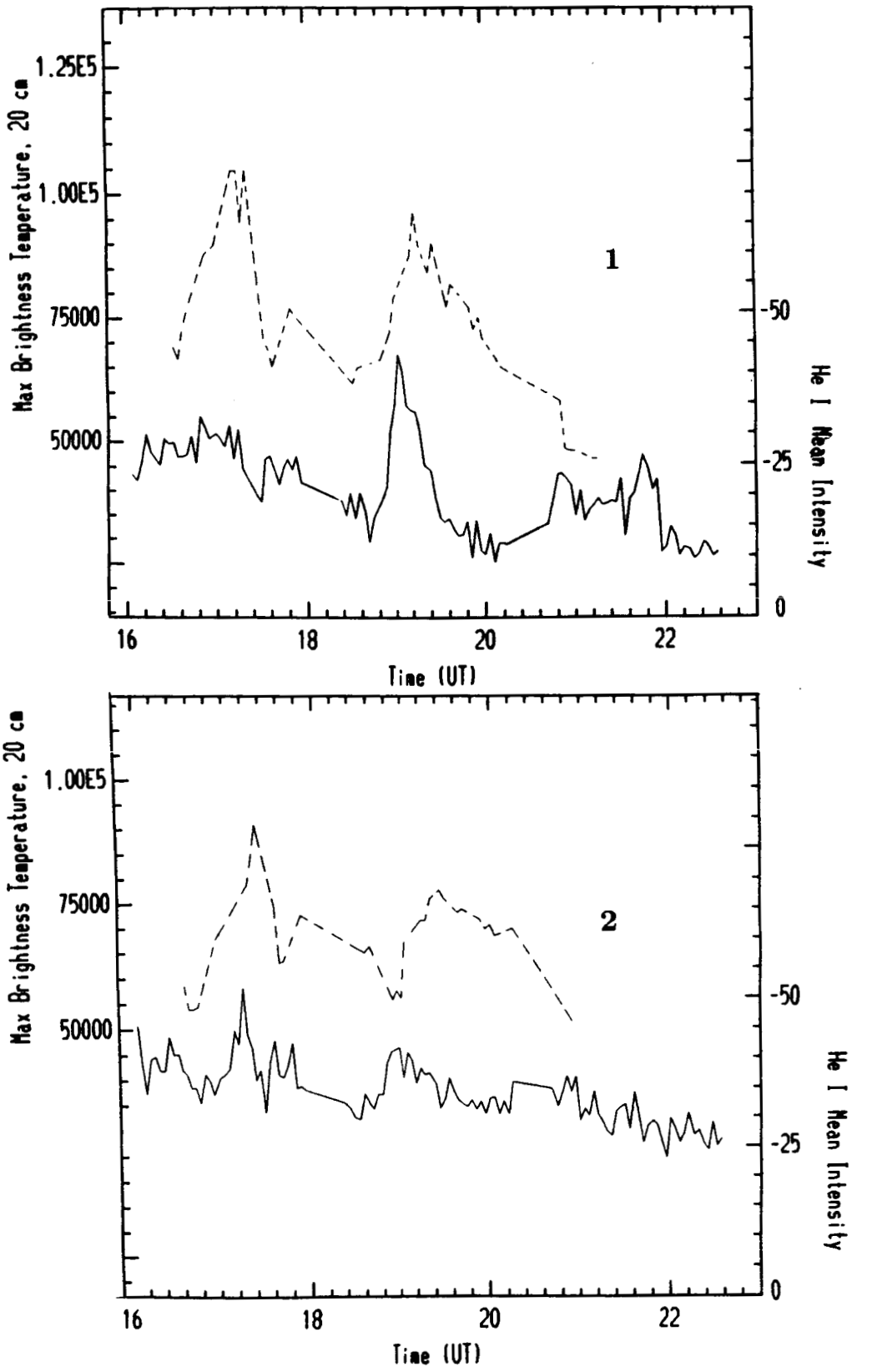
Max Brightness Temperature, 20 cm
1.25E5
1.00E5
75000
50000
1
-50
-25
0
He I Mean Intensity
16
18
20
22
Time (UT)
Max Brightness Temperature, 20 cm
1.00E5
75000
50000
2
-50
-25
0
He I Mean Intensity
16
18
20
22
Time (UT)

Figure 21a

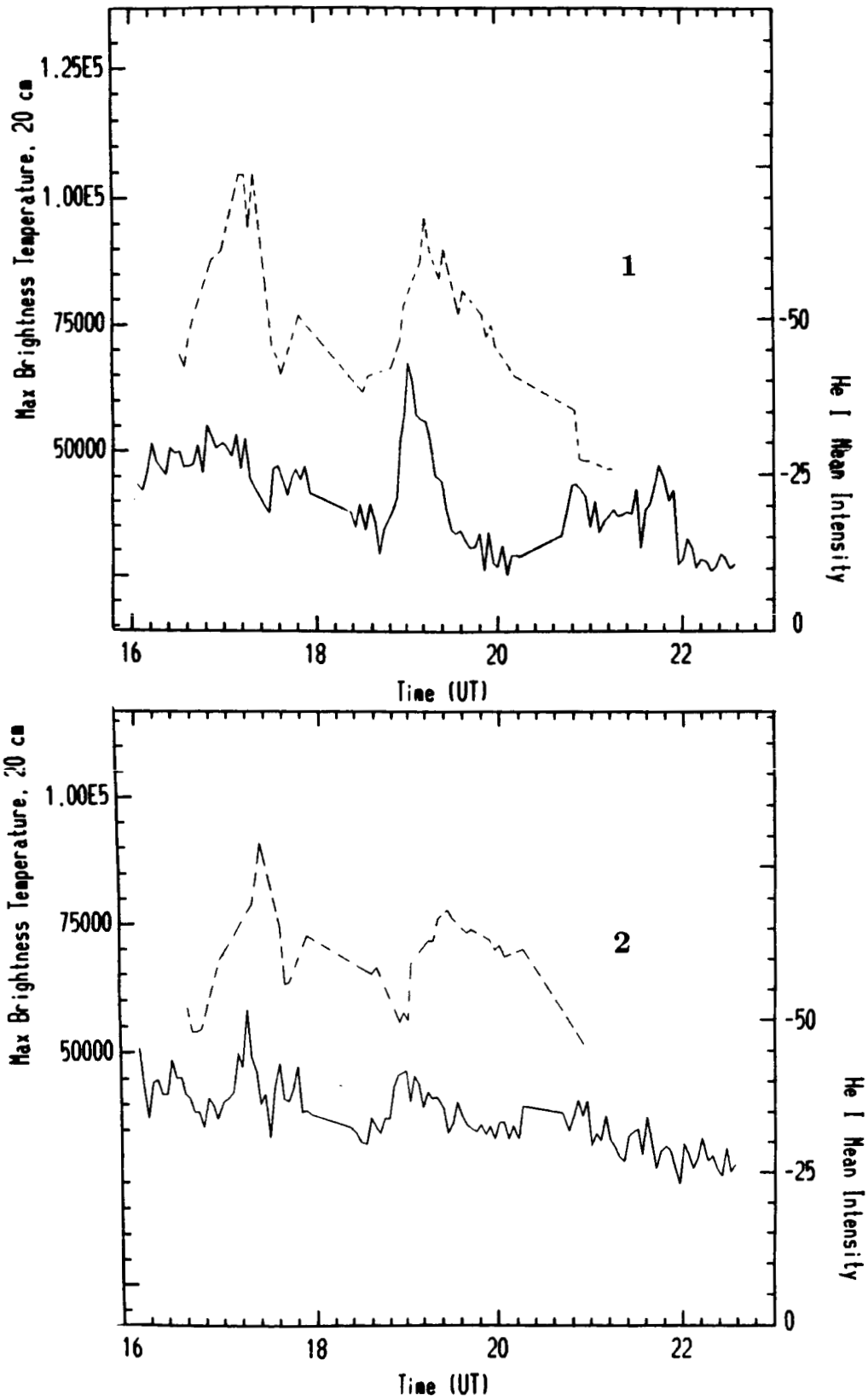
1.25E5
1.00E5
75000
50000
Max Brightness Temperature, 20 cm
1
-50
-25
0
He I Mean Intensity
16
18
20
22
Time (UT)
1.00E5
75000
50000
Max Brightness Temperature, 20 cm
2
-50
-25
0
He I Mean Intensity
16
18
20
22
Time (UT)

Figure 21a

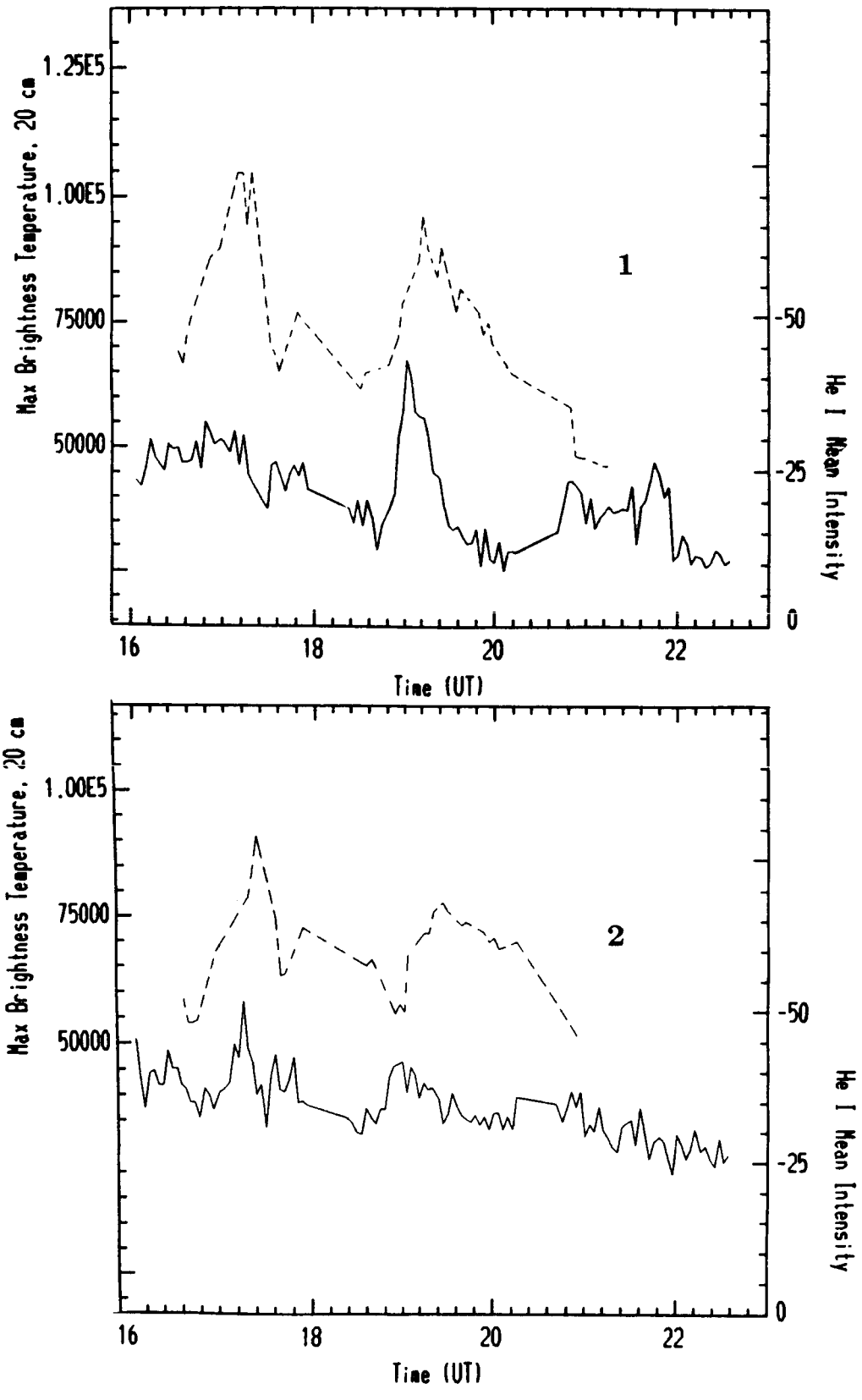
Max Brightness Temperature, 20 cm
1.25E5
1.00E5
75000
50000
1
-50
-25
0
He I Mean Intensity
16
18
20
22
Time (UT)
Max Brightness Temperature, 20 cm
1.00E5
75000
50000
2
-50
-25
0
He I Mean Intensity
16
18
20
22
Time (UT)

Figure 21a

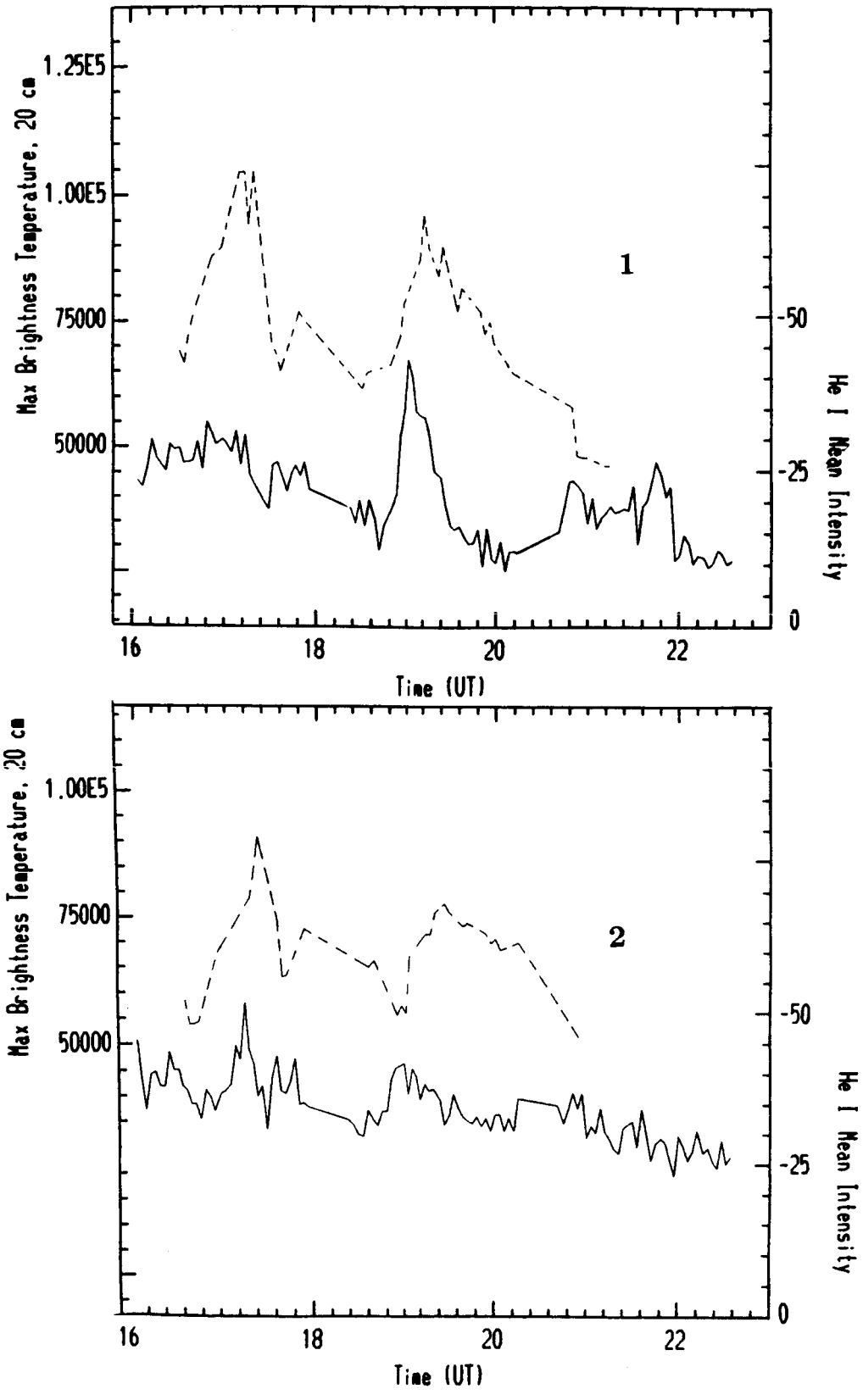
Max Brightness Temperature, 20 cm
1.25E5
1.00E5
75000
50000
1
-50
-25
0
He I Mean Intensity
16
18
20
22
Time (UT)
Max Brightness Temperature, 20 cm
1.00E5
75000
50000
2
-50
-25
0
He I Mean Intensity
16
18
20
22
Time (UT)

Figure 21a

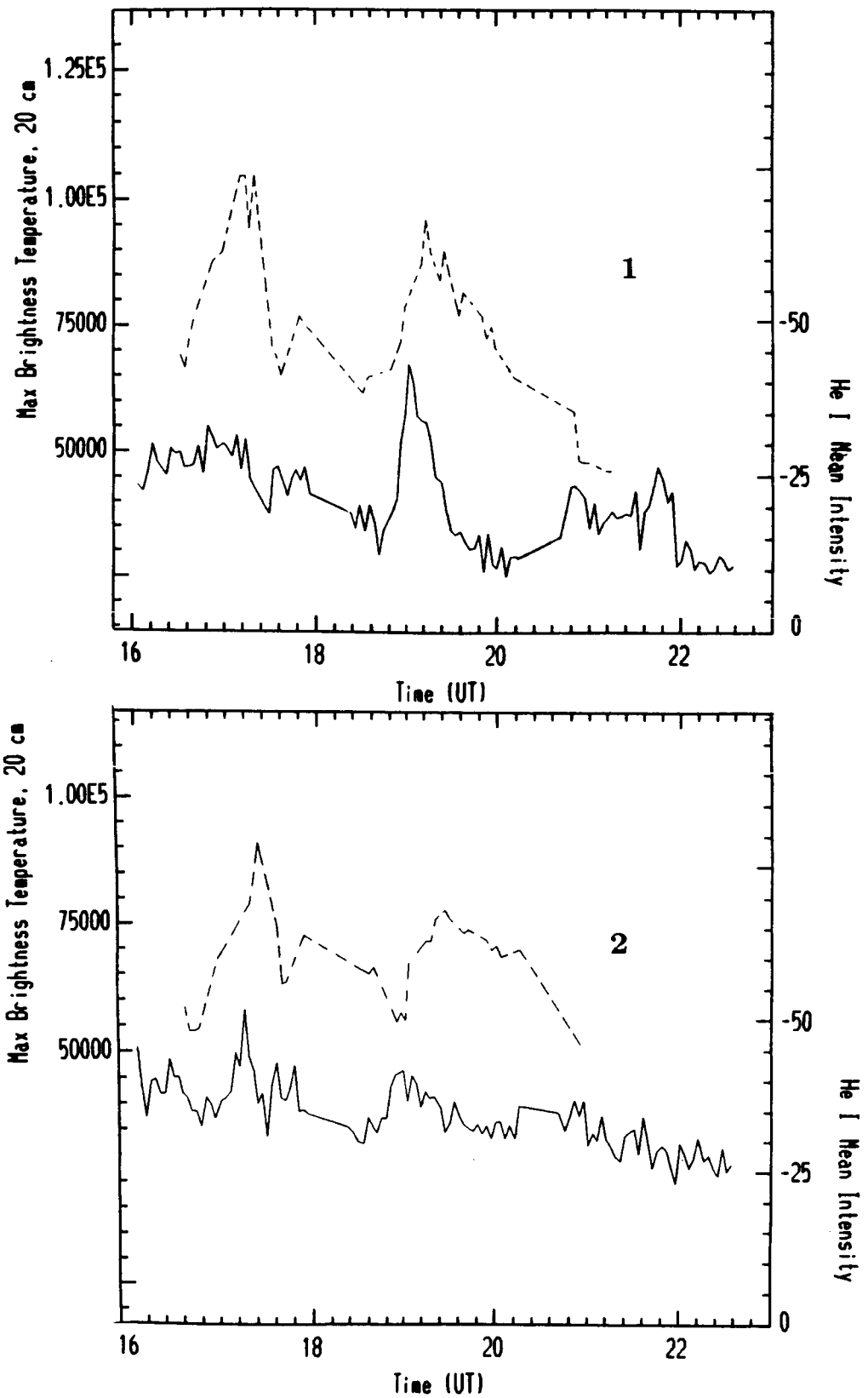
Max Brightness Temperature, 20 cm
1.25E5
1.00E5
75000
50000
1
-50
-25
0
He I Mean Intensity
16
18
20
22
Time (UT)
Max Brightness Temperature, 20 cm
1.00E5
75000
50000
2
-50
-25
0
He I Mean Intensity
16
18
20
22
Time (UT)

Figure 21a

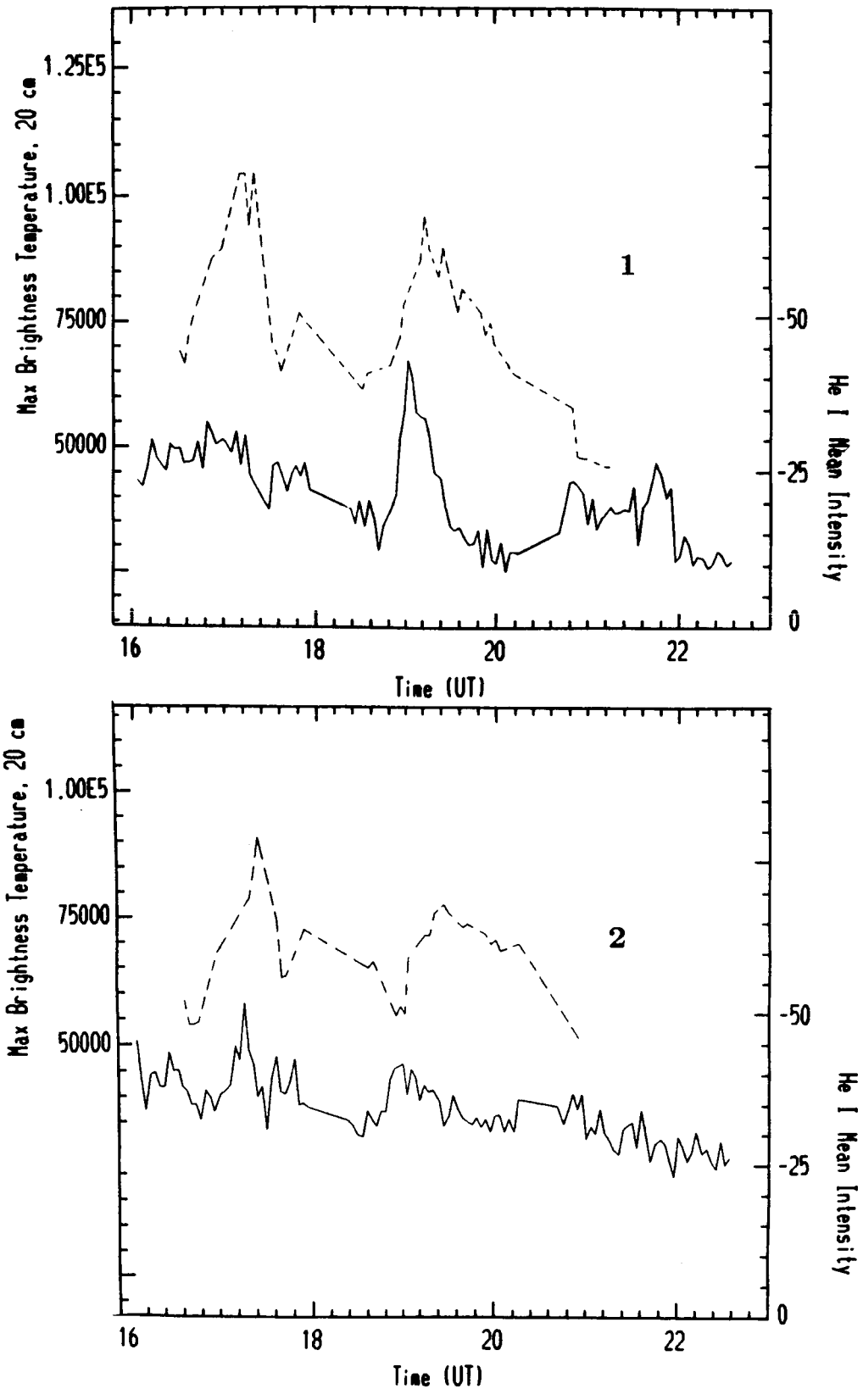
Max Brightness Temperature, 20 cm
1.25E5
1.00E5
75000
50000
1
-50
-25
0
He I Mean Intensity
16
18
20
22
Time (UT)
Max Brightness Temperature, 20 cm
1.00E5
75000
50000
2
-50
-25
0
He I Mean Intensity
16
18
20
22
Time (UT)

Figure 21a

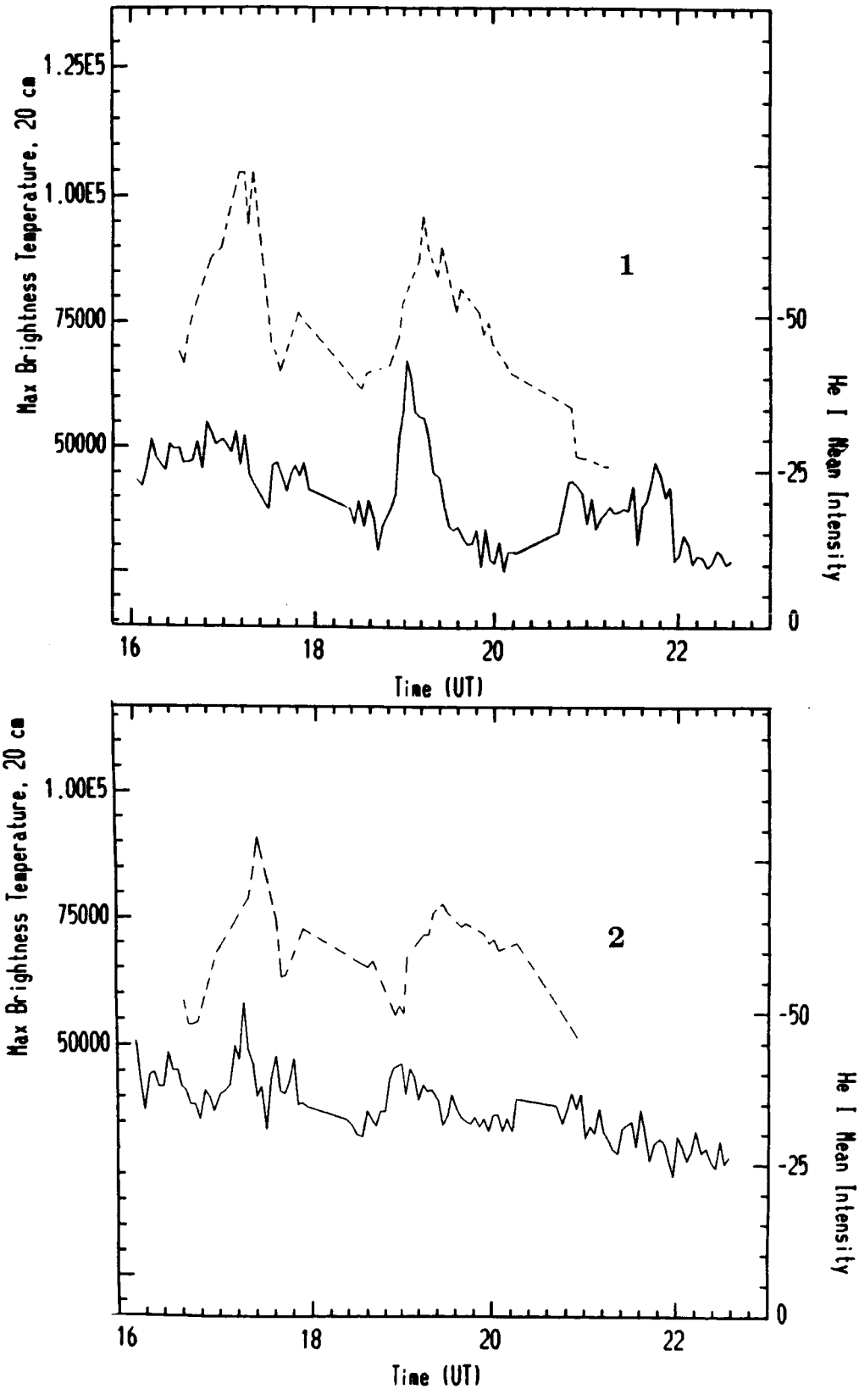
Max Brightness Temperature, 20 cm
1.25E5
1.00E5
75000
50000
1
-50
-25
0
He I Mean Intensity
16
18
20
22
Time (UT)
Max Brightness Temperature, 20 cm
1.00E5
75000
50000
2
-50
-25
0
He I Mean Intensity
16
18
20
22
Time (UT)

Figure 21a

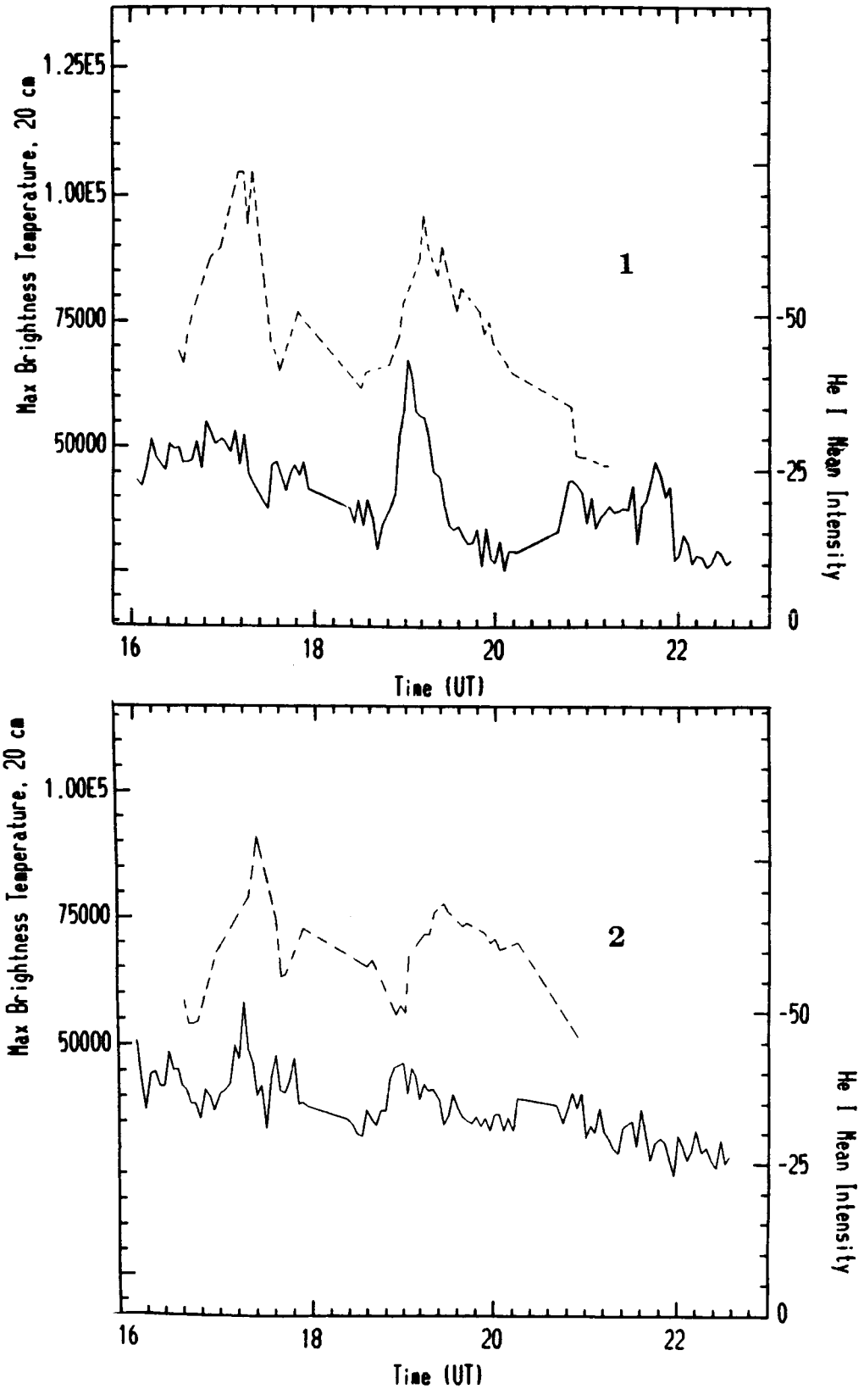
Max Brightness Temperature, 20 cm
1.25E5
1.00E5
75000
50000
1
-50
-25
0
He I Mean Intensity
16
18
20
22
Time (UT)
Max Brightness Temperature, 20 cm
1.00E5
75000
50000
2
-50
-25
0
He I Mean Intensity
16
18
20
22
Time (UT)

Figure 21a

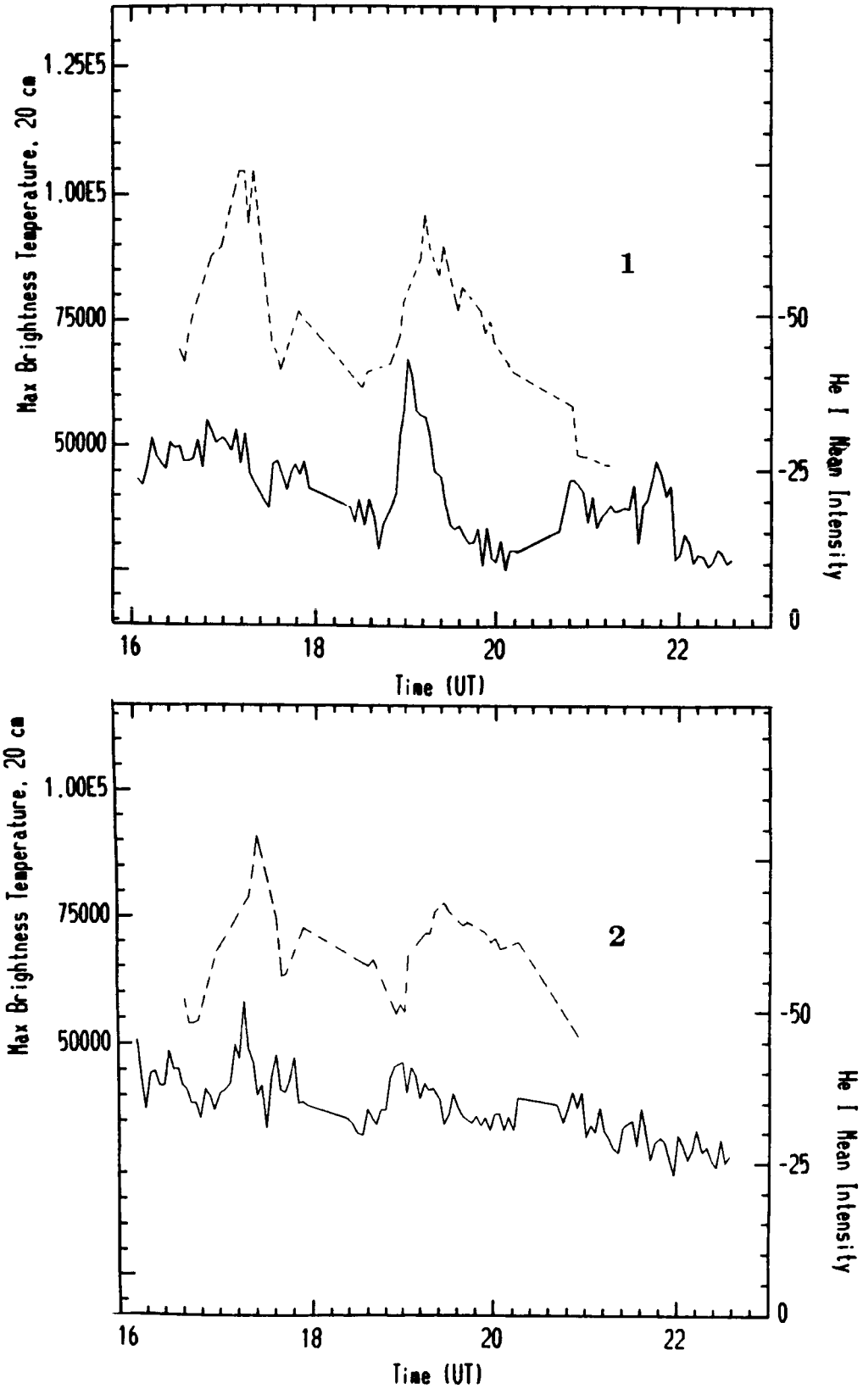
Max Brightness Temperature, 20 cm
1.25E5
1.00E5
75000
50000
1
-50
-25
0
He I Mean Intensity
16
18
20
22
Time (UT)
Max Brightness Temperature, 20 cm
1.00E5
75000
50000
2
-50
-25
0
He I Mean Intensity
16
18
20
22
Time (UT)

Figure 21a

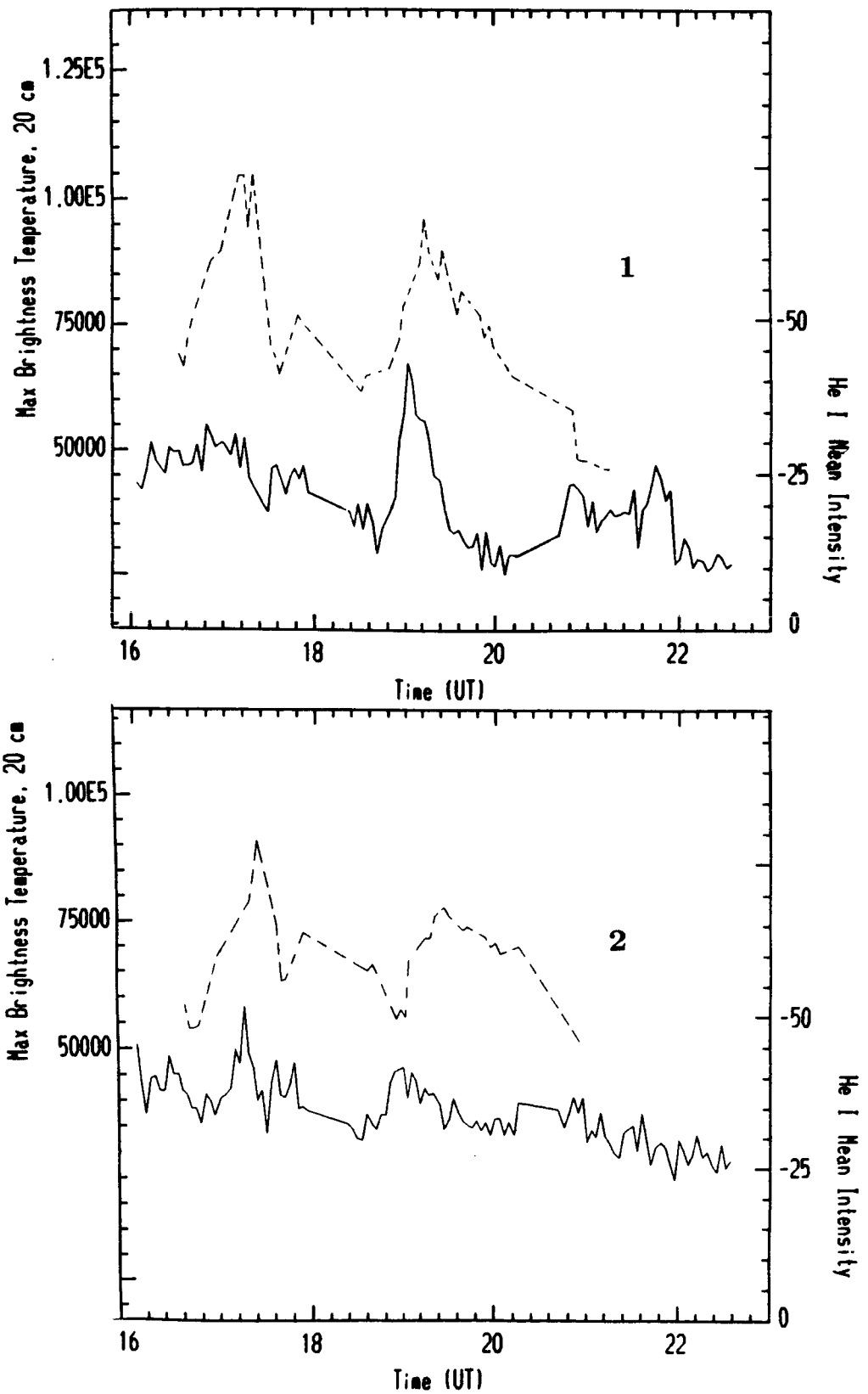
Max Brightness Temperature, 20 cm
1.25E5
1.00E5
75000
50000
1
-50
-25
0
He I Mean Intensity
16
18
20
22
Time (UT)
Max Brightness Temperature, 20 cm
1.00E5
75000
50000
2
-50
-25
0
He I Mean Intensity
16
18
20
22
Time (UT)

Figure 21a

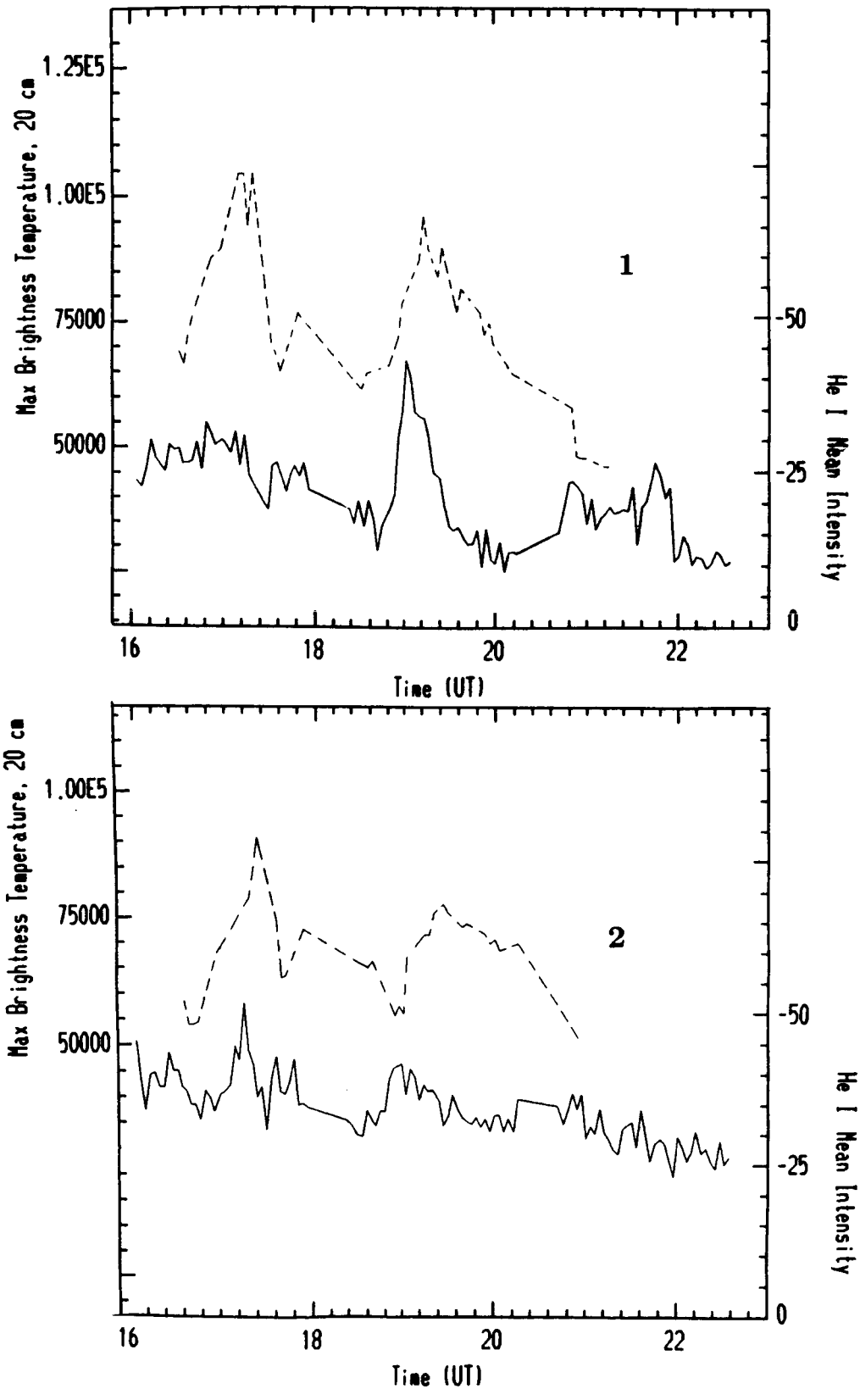
Max Brightness Temperature, 20 cm
1.25E5
1.00E5
75000
50000
1
-50
-25
0
He I Mean Intensity
16
18
20
22
Time (UT)
Max Brightness Temperature, 20 cm
1.00E5
75000
50000
2
-50
-25
0
He I Mean Intensity
16
18
20
22
Time (UT)

Figure 21a

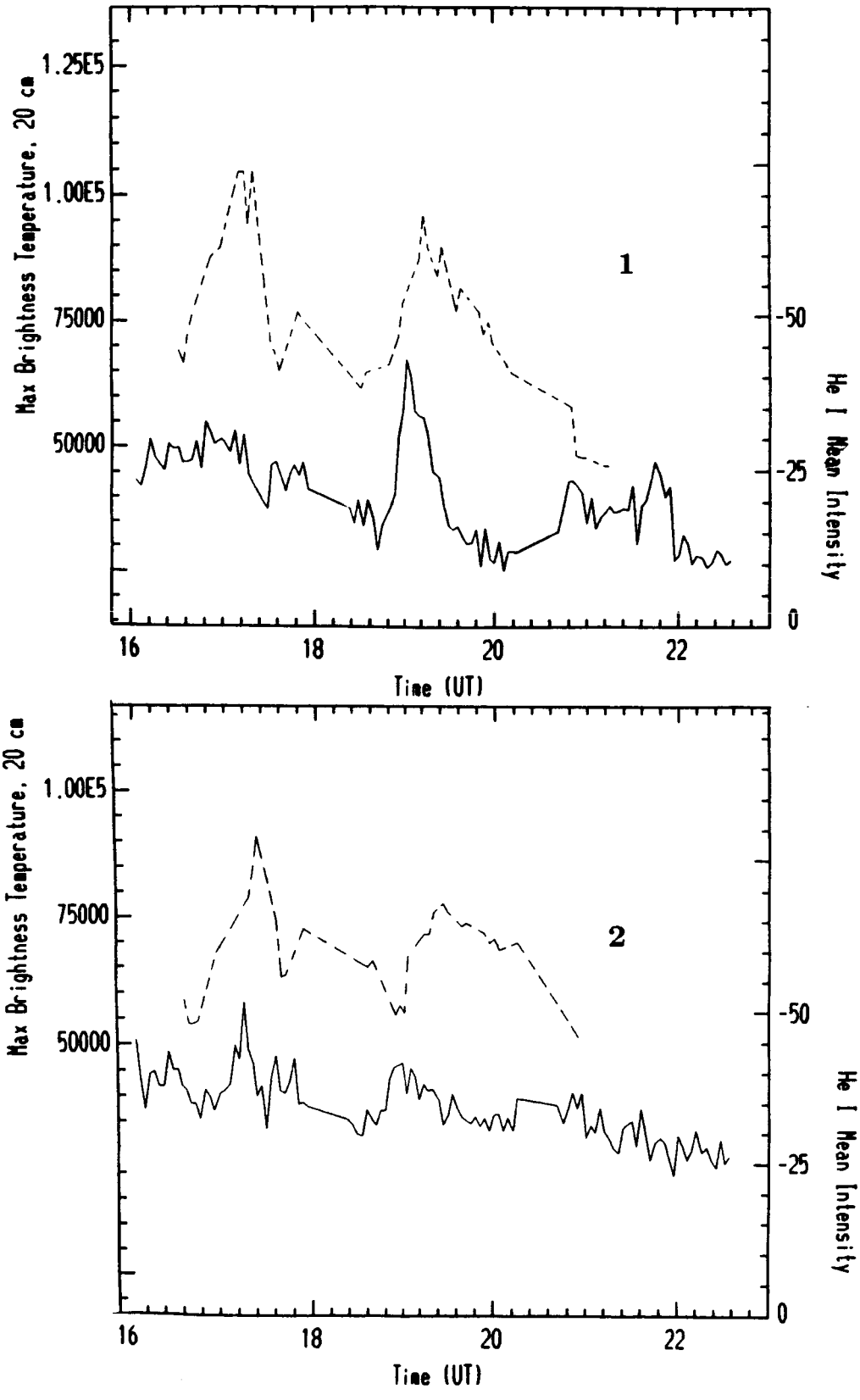
1.25E5
1.00E5
75000
50000
Max Brightness Temperature, 20 cm
1
-50
-25
0
He I Mean Intensity
16
18
20
22
Time (UT)
1.00E5
75000
50000
Max Brightness Temperature, 20 cm
2
-50
-25
0
He I Mean Intensity
16
18
20
22
Time (UT)

Figure 21a

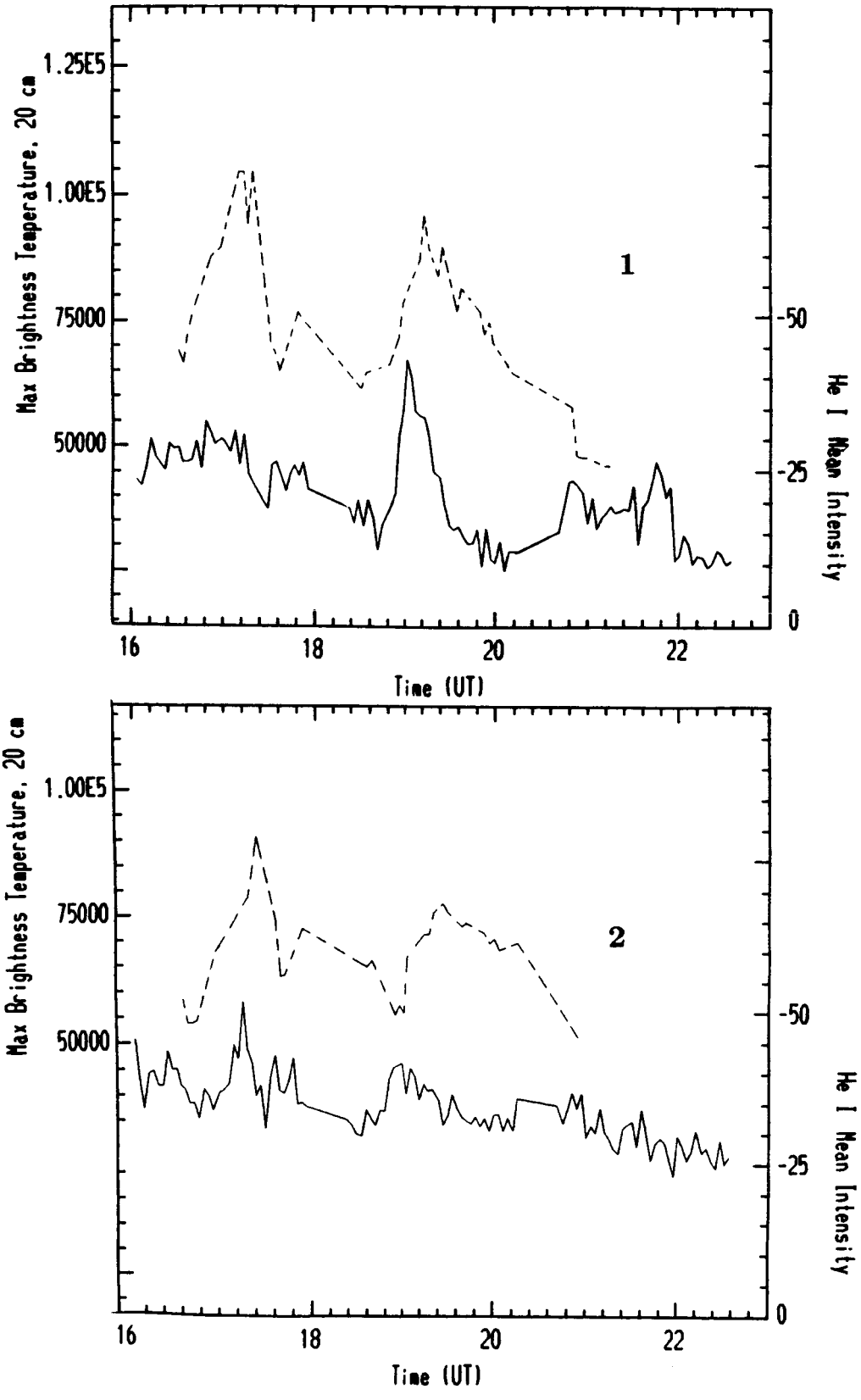
1.25E5
1.00E5
75000
50000
Max Brightness Temperature, 20 cm
1
-50
-25
0
He I Mean Intensity
16
18
20
22
Time (UT)
1.00E5
75000
50000
Max Brightness Temperature, 20 cm
2
-50
-25
0
He I Mean Intensity
16
18
20
22
Time (UT)

Figure 21a

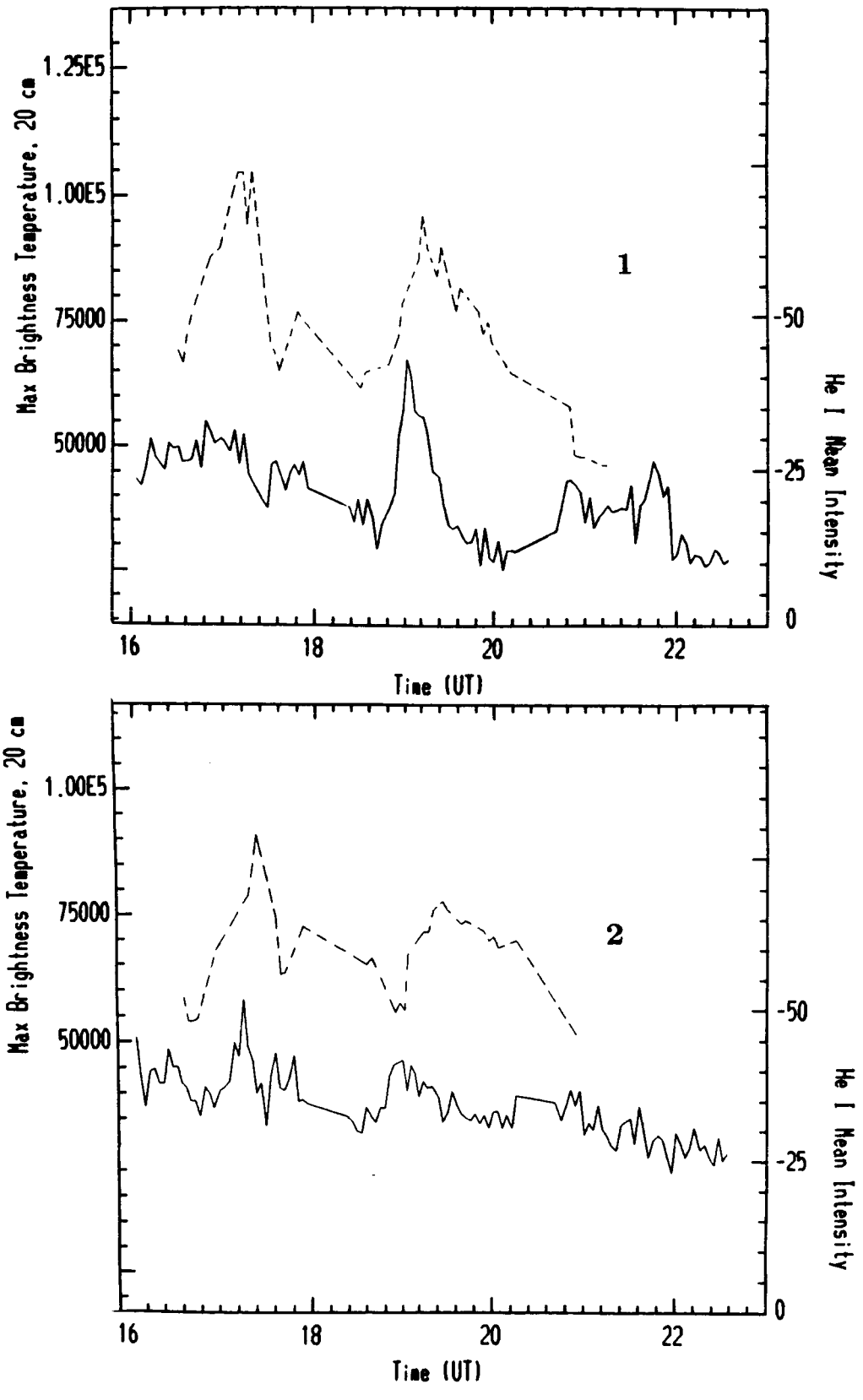
1.25E5
1.00E5
75000
50000
Max Brightness Temperature, 20 cm
1
-50
-25
0
He I Mean Intensity
16
18
20
22
Time (UT)
1.00E5
75000
50000
Max Brightness Temperature, 20 cm
2
-50
-25
0
He I Mean Intensity
16
18
20
22
Time (UT)

Figure 21a

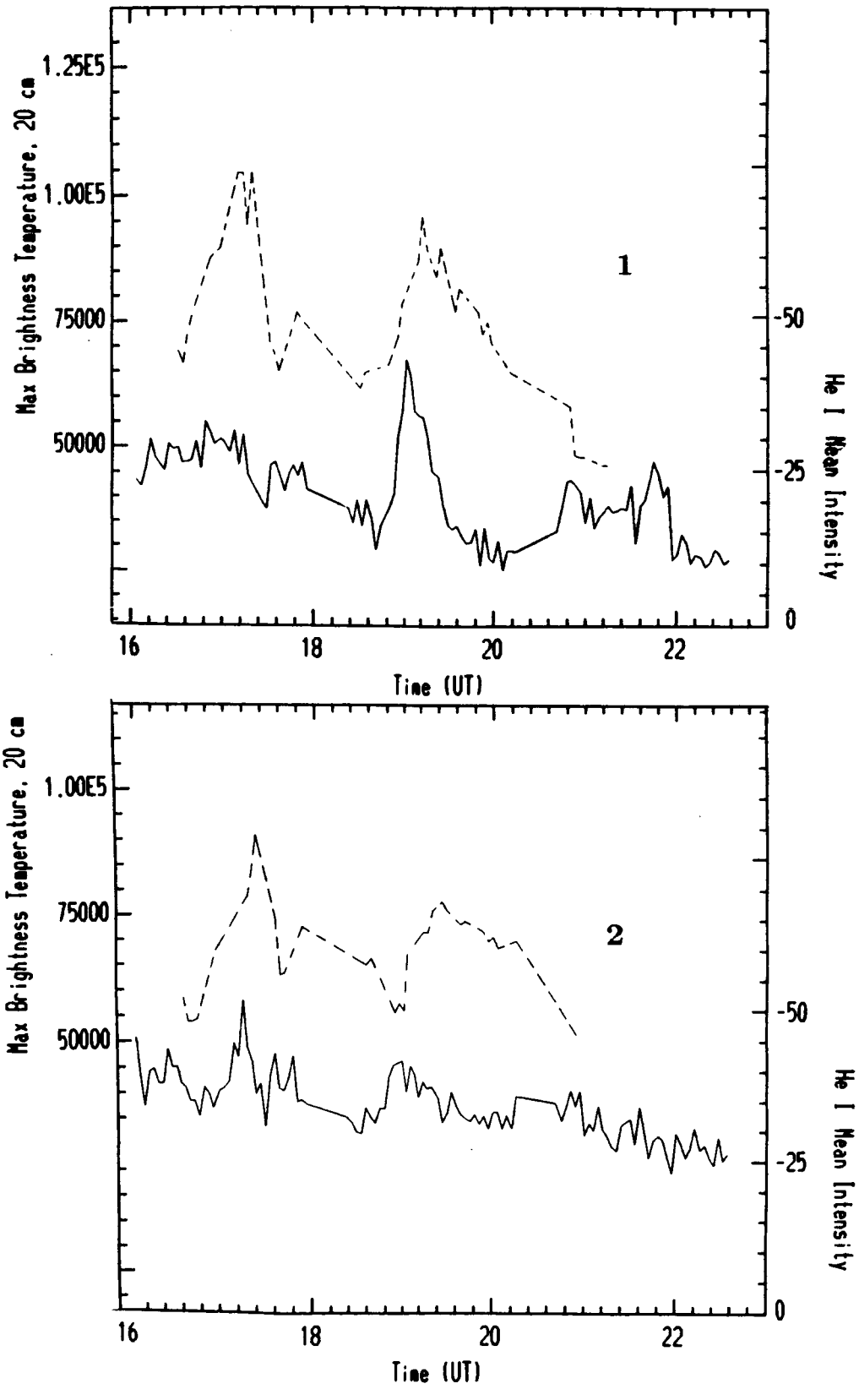
Max Brightness Temperature, 20 cm
1.25E5
1.00E5
75000
50000
1
-50
-25
0
He I Mean Intensity
16
18
20
22
Time (UT)
Max Brightness Temperature, 20 cm
1.00E5
75000
50000
2
-50
-25
0
He I Mean Intensity
16
18
20
22
Time (UT)

Figure 21a

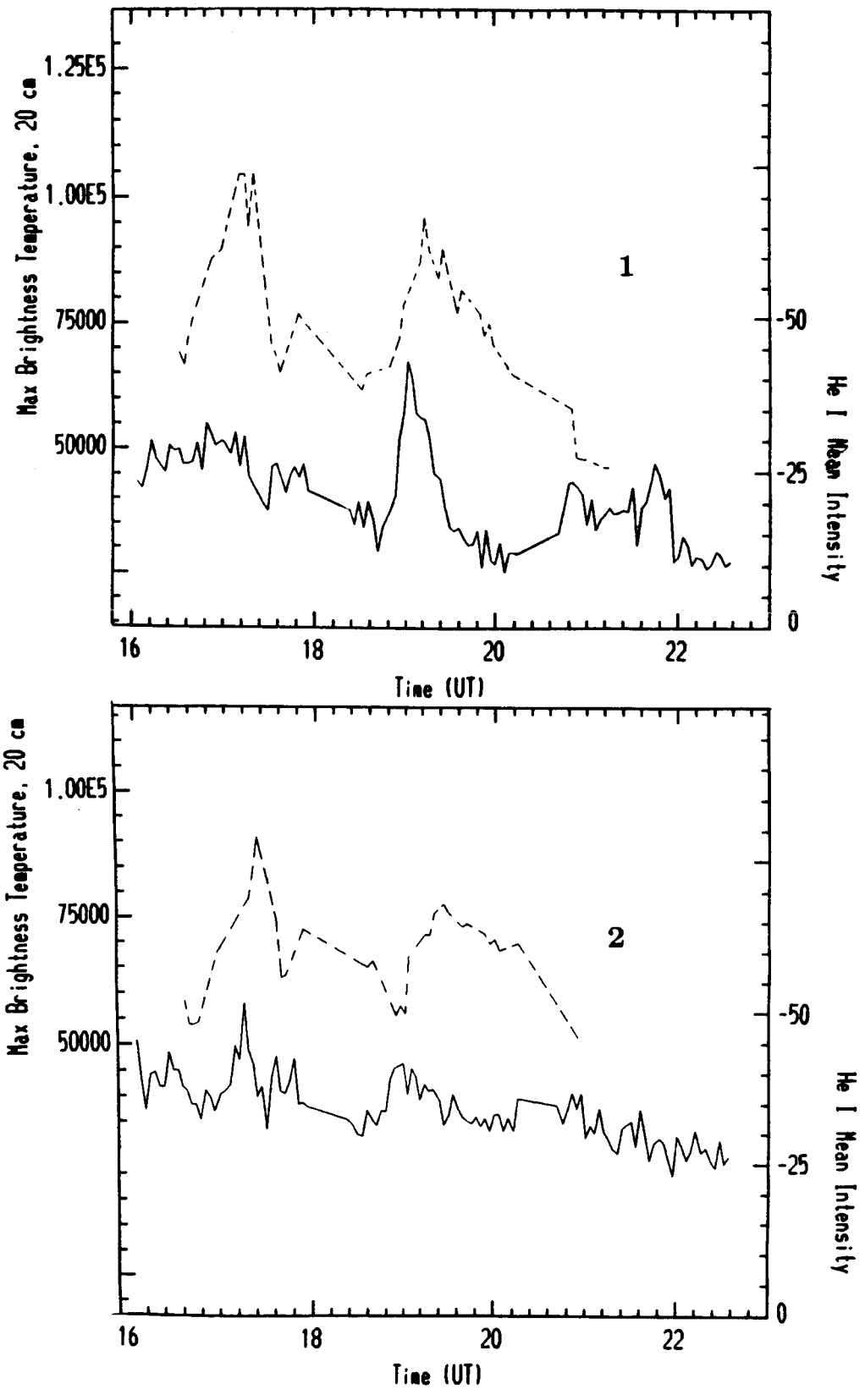
Max Brightness Temperature, 20 cm
1.25E5
1.00E5
75000
50000
1
-50
-25
0
He I Mean Intensity
16
18
20
22
Time (UT)
Max Brightness Temperature, 20 cm
1.00E5
75000
50000
2
-50
-25
0
He I Mean Intensity
16
18
20
22
Time (UT)

Figure 21a

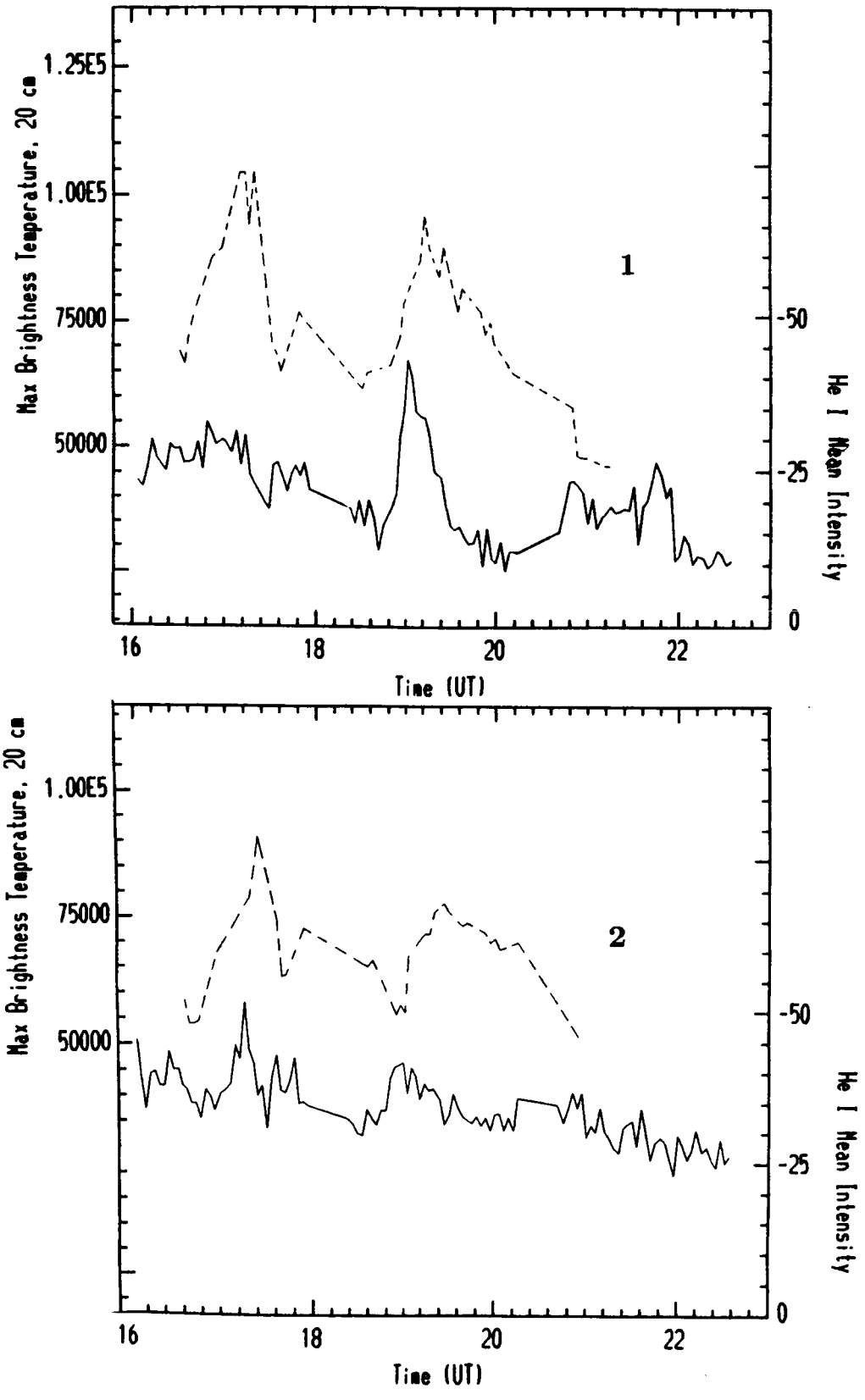
Max Brightness Temperature, 20 cm
1.25E5
1.00E5
75000
50000
1
-50
-25
0
He I Mean Intensity
16
18
20
22
Time (UT)
Max Brightness Temperature, 20 cm
1.00E5
75000
50000
2
-50
-25
0
He I Mean Intensity
16
18
20
22
Time (UT)

Figure 21b

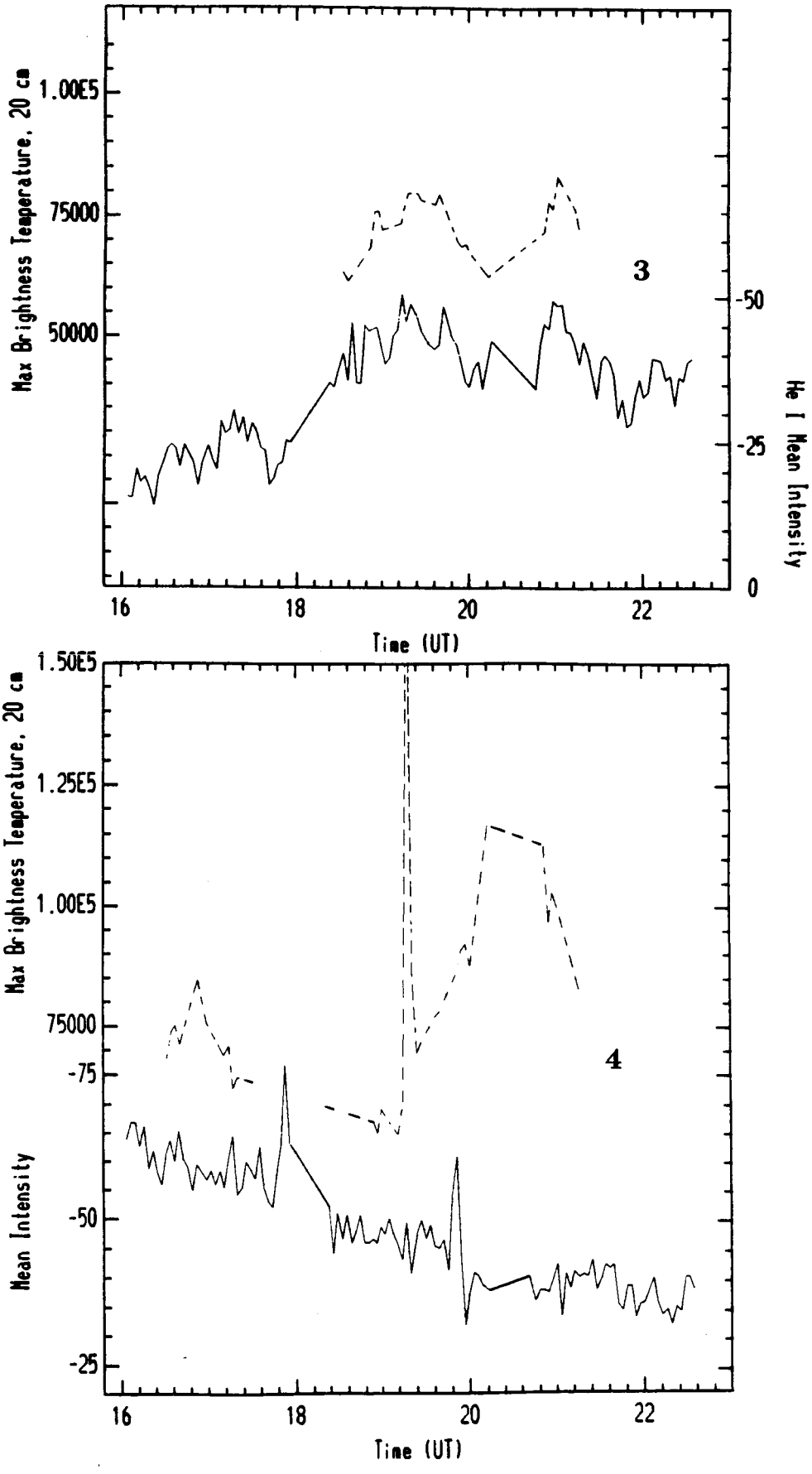
Max Brightness Temperature, 20 cm
1.00E5
75000
50000
3
-50
-25
0
He I Mean Intensity
16
18
20
22
Time (UT)
Max Brightness Temperature, 20 cm
1.50E5
1.25E5
1.00E5
75000
-75
-50
-25
Mean Intensity
4
16
18
20
22
Time (UT)

Figure 21b

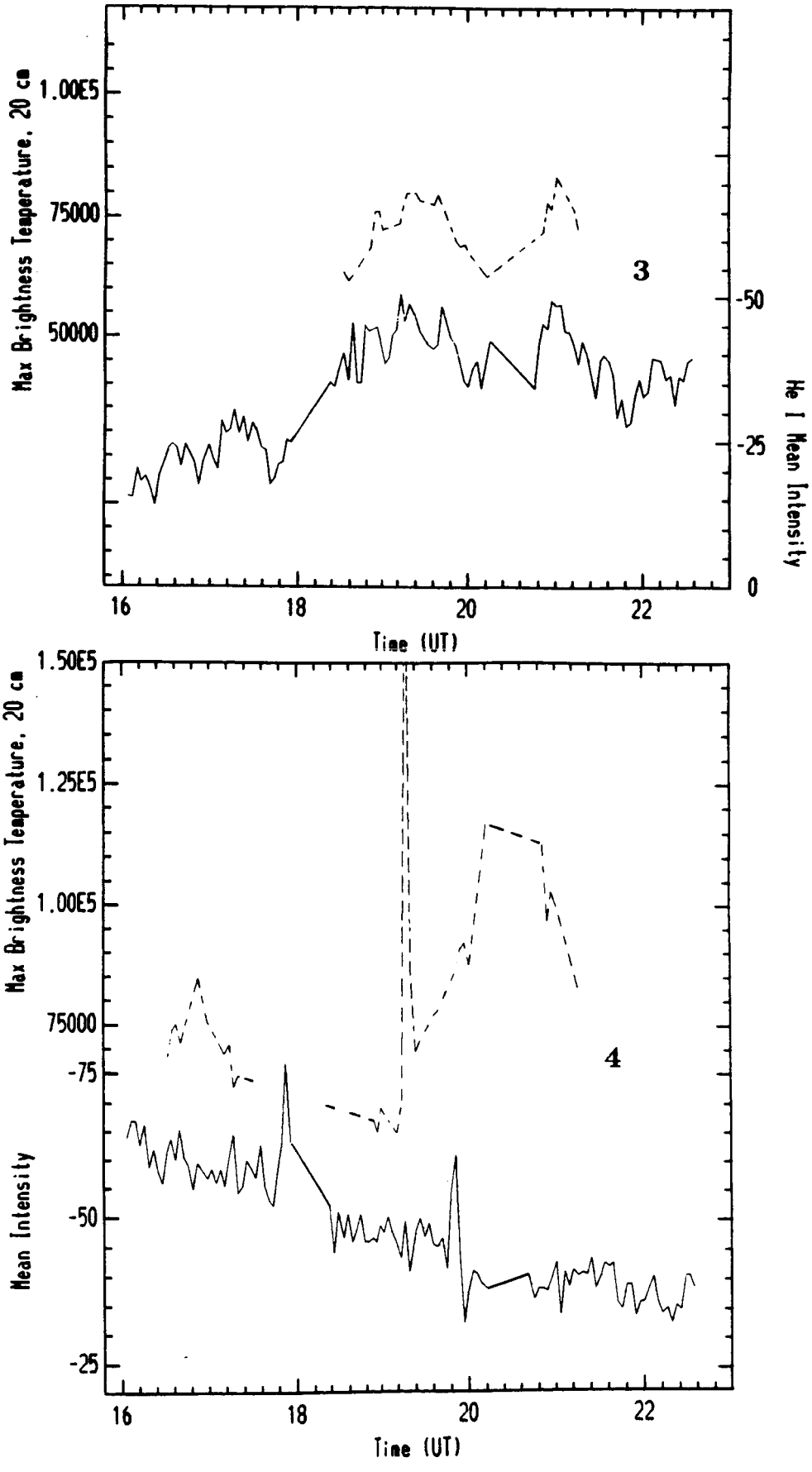
Max Brightness Temperature, 20 cm
1.00E5
75000
50000
3
-50
-25
0
He I Mean Intensity
16
18
20
22
Time (UT)
Max Brightness Temperature, 20 cm
1.50E5
1.25E5
1.00E5
75000
-75
-50
-25
4
Mean Intensity
16
18
20
22
Time (UT)